

Review

Recent and Emerging Trends in Remediation of Methylene Blue Dye from Wastewater by Using Zinc Oxide Nanoparticles

Shreya Modi ^{1,†}, Virendra Kumar Yadav ^{2,†} , Amel Gacem ³ , Ismat H. Ali ⁴ , Dhruv Dave ⁵,
Samreen Heena Khan ⁶, Krishna Kumar Yadav ⁷ , Sami-ullah Rather ⁸ , Yongtae Ahn ⁹ , Cao Truong Son ^{10,*} 
and Byong-Hun Jeon ^{9,*} 

- ¹ Department of Microbiology, Shri Sarvajanic Science College, Mehsana 384001, India; shreyamodi20@gmail.com
- ² Department of Biosciences, School of Liberal Arts and Sciences, Mody University, Lakshmanagarh, Sikar 332311, Rajasthan, India; yadava94@gmail.com
- ³ Department of Physics, Faculty of Sciences, University 20 Août, Skikda 1955, Algeria; gacem_amel@yahoo.fr
- ⁴ Department of Chemistry, College of Science, King Khalid University, P.O. Box 9004, Abha 61413, Saudi Arabia; ihali@kku.edu.sa
- ⁵ Department of Life sciences, Hemchandracharya North Gujarat University, Patan 384265, India; redgarden2009@gmail.com
- ⁶ Department of Research and Development, YNC Envis Pvt Ltd., Delhi 110059, India; samreen.heena.khan@gmail.com
- ⁷ Faculty of Science and Technology, Madhyanchal Professional University, Ratibad, Bhopal 462044, India; envirokrishna@gmail.com
- ⁸ Department of Chemical and Materials Engineering, King Abdulaziz University, P.O. Box 80204, Jeddah 21589, Saudi Arabia; rathersami@kau.edu.sa
- ⁹ Department of Earth Resources & Environmental Engineering, Hanyang University, 222-Wangsimni-ro, Seongdong-gu, Seoul 04763, Korea; ytahn83@hanyang.ac.kr
- ¹⁰ Faculty of Natural Resources and Environment, Vietnam National University of Agriculture, Hanoi 100000, Vietnam
- * Correspondence: caotruongson.hua@gmail.com (C.T.S.); bhjeon@hanyang.ac.kr (B.-H.J.)
- † These authors contributed equally to this work.



Citation: Modi, S.; Yadav, V.K.; Gacem, A.; Ali, I.H.; Dave, D.; Khan, S.H.; Yadav, K.K.; Rather, S.-u.; Ahn, Y.; Son, C.T.; et al. Recent and Emerging Trends in Remediation of Methylene Blue Dye from Wastewater by Using Zinc Oxide Nanoparticles. *Water* **2022**, *14*, 1749. <https://doi.org/10.3390/w14111749>

Academic Editor: Constantinos V. Chrysikopoulos

Received: 31 March 2022

Accepted: 24 May 2022

Published: 29 May 2022

Publisher's Note: MDPI stays neutral with regard to jurisdictional claims in published maps and institutional affiliations.



Copyright: © 2022 by the authors. Licensee MDPI, Basel, Switzerland. This article is an open access article distributed under the terms and conditions of the Creative Commons Attribution (CC BY) license (<https://creativecommons.org/licenses/by/4.0/>).

Abstract: Due to the increased demand for clothes by the growing population, the dye-based sectors have seen fast growth in the recent decade. Among all the dyes, methylene blue dye is the most commonly used in textiles, resulting in dye effluent contamination. It is carcinogenic, which raises the stakes for the environment. The numerous sources of methylene blue dye and their effective treatment procedures are addressed in the current review. Even among nanoparticles, photocatalytic materials, such as TiO₂, ZnO, and Fe₃O₄, have shown greater potential for photocatalytic methylene blue degradation. Such nano-sized metal oxides are the most ideal materials for the removal of water pollutants, as these materials are related to the qualities of flexibility, simplicity, efficiency, versatility, and high surface reactivity. The use of nanoparticles generated from waste materials to remediate methylene blue is highlighted in the present review.

Keywords: photocatalytic; effluents; auxochrome; polyvinylpyrrolidone; hazardous amines

1. Introduction

The contamination of water is a severe ecological concern and a threat to the climate's perfect balance [1]. The dumping of wastewater into natural water resources has also grown as a result of growing development. One of the pollutants found in wastewater is dye, which is widely used in a variety of industries, including textiles, food, and paper [2]. According to the color index, there are currently over 10,000 different types of dyes accessible around the globe, with over 700,000 tonnes produced annually [3]. Every year, over 2×10^5 tons of dyes are released as effluents during dyeing and finishing operations in the textile sector, due to the ineffectiveness of the dyeing process [4]. Because of their

color, high chemical oxygen demand (COD), and extremely complex chemical makeup, industrially released effluents pose significant environmental risks [5]. Light, temperature, water, chemicals, detergents, soap, and other variables, such as bleach and perspiration, have little effect on these colors. Dyes are not well treated by wastewater treatment, and they stay in the environment for prolonged periods [6]. Antimicrobial compounds are resistant to biodegradation due to their synthetic origin and complex character [7]. Most dyes are poisonous and can cause carcinogenic, mutagenic, teratogenic, and other detrimental effects on fish species and microbial diversity [8]. They can also harm humans by causing damage to the brain, central nervous system, and reproductive system [8]. Benzidine and other aromatic chemicals are used in several dyes, which are recognized carcinogens. Certain azo and nitro group chemicals are reported to be reduced in sediments and the intestinal environment, resulting in the formation of hazardous amines [9]. Because a dye concentration of 1 ppm in drinking water might render it unsafe for human consumption, dye removal is critical [10].

Dyes are organic mixtures that can connect themselves to the surface of fabrics or materials to give vibrant and long-lasting color [11]. They can be natural or synthetic. A mordant may be required for dyes to improve the dye's speed on the substance to which it is applied. Plants have evolved the most dyes, particularly various roots, berries, bark, leaves, and wood, but only a few are commonly utilized on a commercial basis [12].

Coal tar yields benzene, naphthalene, phenol, aniline, and other compounds that are utilized as starting materials in the manufacture of synthetic colors (Seow and Lim 2016). Textiles, paper, dyeing, and plastics are just a few of the industries that employ various dyes to color their products and require a significant quantity of water [13]. They produce a significant volume of colored waste effluent. It is widely acknowledged that the color of water has a significant impact on public perceptions of water quality. Color is the first pollutant discovered in wastewater. The presence of a small number of dyes in water is very obvious, traceable, and unfavorable [14]. Dyestuff industrial effluents are one of the most difficult wastewaters to treat, not only because of their high chemical oxygen demand (COD), but also because of other factors, such as suspended particles, turbidity, hazardous components, and color [15]. Because of the presence of metals, aromatics, and other compounds in dyes, they may have an impact on aquatic life. Dyes are usually synthetic and have a complex aromatic molecular structure, making them more stable and difficult to biodegrade [16].

A dye is made up of two sorts of components: chromophores and auxochromes. Color is imparted to substances through chromophores, which are unsaturated groups. Nitro ($-\text{NO}_2$), azo ($-\text{N}=\text{N}-$), alkene ($>\text{C}=\text{C}$), and other chromophores are important. Chromogens are substances that include chromophores. While auxochrome is a dye that should be light, water, and soap resistant, it must be connected to the fibers through chemical bonds that are stable [17].

2. Methylene Blue Dye

Methylene blue (MB) is a heterocyclic basic dye with a molecular weight of 373.9 g/mol and a maximum wavelength of 665 nm [18]. Basic blue (9) is its scientific name, and its molecular formula is $\text{C}_{16}\text{H}_{18}\text{N}_3\text{SCl}$ (Farouk 2018); Figure 1 depicts the chemical structure of MB dye. The cationic MB dye is more poisonous than anionic dyes [19]. Textile, rubber, plastics, leather, cosmetics, pharmaceuticals, and food sectors are just a few of the industries that employ MB [20]. Dye residues can be found in industrial effluents discharged by such industrial activities. As a result, the presence of extremely lower quantities in the effluent is readily apparent [4].

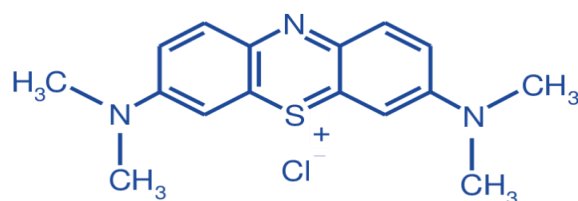


Figure 1. Chemical structure of methylene blue dye.

2.1. Health Impact of MB

MB is a basic and cationic dye that is widely utilized in clinical medicine as a colorant, indicator, and antibacterial chemical [4]. Cancer, mutation, hemolytic anemia, hyperbilirubinemia, chromosomal failure, pulmonary toxicity, and acute renal failure are all linked to MB dye. In SK-N-MC human neuroblastoma and U-373 MG human astrocytoma cells, a microgram level of MB is said to induce cytotoxicity [21]. MB's oral median lethal dosage (LD50) was calculated to be 1180 mg kg^{-1} . It has also been reported that during endotoxemia, low and moderate dosages of MB increase arterial blood pressure, whereas high doses worsen systemic hypotension, myocardial depression, and hypertension [22]. The effects of a high dose of MB on renal and mesenteric blood flow increase vascular resistance and deteriorate gas exchange. It also causes self-limiting greenish-blue urine and a bluish area of skin and mucosa [23].

An incident of skin and fat corruption followed by dry gangrene of the skin in a female patient with breast cancer who underwent sentinel lymph node biopsy limiting utilizing the peri-tumoral infusion of MB color was accounted for as a result of its tissue receptive qualities [24]. Silva et al. (2021) also reported the MB dye effect on hemodynamic and metabolic response in patients of septic shock [25]. The findings of the pulse oximeter's light emission are obstructed by MB, resulting in an erroneously low oxygen saturation measurement. MB also interacts with dapsone to produce hydroxylamine, which causes hemolysis by oxidizing hemoglobin [26]. Because of its ability to inhibit monoamine oxidase (MAO), MB can produce lethal serotonin poisoning at levels greater than 5 mg/kg and rarely causes severe anaphylactic shock. It is virtually completely contraindicated in G6PD deficient patients since it can cause severe hemolysis, as well as in people with Heinz body anemia [27].

2.2. Environmental Impact of MB

Dyes pose several environmental and health risks due to their great thermal and photo-stability, as well as their resistance to biodegradation, as dyes can be left in the environment for longer periods. The absorption and reflection of solar light into the aquatic body is the major environmental concern with dyes. Many aspects of algal growth are affected by the presence of an increasing amount of dye in a water body, including protein content, pigment content, and other nutrient content [28,29].

There are several reports where MB from the disposed sites could reach up to the water bodies and affect the other microbial communities residing over there. For instance, Moorthy et al. (2021) reported the acute toxicity of textile MB on the metabolism and growth of some of the selected freshwater microalgae. When *Chlorella vulgaris* and *Spirulina platensis* were exposed to MB, there was acute toxicity. The toxicity resulted in the growth inhibition rate, inhibition of pigment and protein content.

3. Industrial Dye Effluent Treatment

Dye-containing effluent is generated as a result of the industry's massive application. However, because it has been identified and targeted by federal legislation, it is increasingly common to carry out studies on the various techniques of treatment and application of dyes within the dyeing sector [30]. For the treatment of dyes, a variety of traditional procedures have been used, which can be broadly categorized into conventional treatment process (CTP), established recovery process, and emerging removal process (ERP). CTP involves

coagulation-based and flocculants-based biodegradation and adsorption. While the established recovery process involves membrane separation, ion exchange and oxidation. The ERP indulges in an advanced oxidation process (AOPs), biomass-based remediation, and selective bio sorbent-based remediation. All these techniques have their pros and cons [31].

The strategies stated above are quite successful and significant, but they have some limitations in terms of applicability, cost, efficacy, and time. The usage of these procedures also results in secondary contamination. As a result, scientists must seek out a replacement strategy for the complete breakdown of organic contaminants and dyes.

Pirkarami and Olya 2017, conducted a study on color removal from wastewater in 2017. They also looked at the effects of varied current density, anode type, temperature, pH, and electrolyte concentration factors on the removal of Reactive Red 120 from synthetic wastewater. Researchers that used the optimal conditions to treat real textile dyestuff waste effluents did not achieve the desired outcomes. GC-MS analysis was used to characterize the product obtained following post-treatment. The dye removal process in real dye waste effluent is more complex than in manufactured wastewater, according to the researchers.

MB dyes have a long history of application in both industry and medicine. However, excessive exposure poses a health risk and has a negative influence on the environment [32]. For MB dye removal and degradation, a range of adsorbents, chemicals, biosorbents, and microorganisms have been tested, which is provided in Table 1 [33–49].

Table 1. Removal proficiency of different adsorbents/reagent/bio sorbents for the evacuation of MB dye.

Reagent/Adsorbent	Type	Removal %	Reference
1-4 Fe Electrode	Electrocoagulation	100%	[33]
Fe electrode	Electrocoagulation	80%	[34]
Al and stainless steel	Electrocoagulation in couple	99%	[35]
Hydrogen peroxide	Oxidation	86%	[36]
Bentonite Clay	Natural	99.9%	[37]
Teak Tree Bark powder	Natural	33%	[37]
HDTMA clay (surfactant modified)	Natural	30%	[38]
HDPy-Clay (surfactant modified)	Natural	29%	[38]
Guava peel	Natural	19%	[39]
Jack fruit peel	Natural	29%	[40]
Broad Bean peel	Natural	19%	[41]
Pineapple stem	Natural	12%	[42]
Algerian clay	Natural	65	[43]
NaOH treated rice husk	Agriculture	4%	[44]
Xylene with benzoic acid	Surfactant	99%	[45]
SDBS/amyl alcohol	Surfactant	98%	[46]
AOT/amyl alcohol	Surfactant	97%	[46]
Toluene (extractant) benzoic acid	Surfactant	95%	[45]
Parthenium hysterophorus weed (untreated)	Biosorbent	2.4%	[47]
<i>Aspergillus fumigates</i>	Fungi	80%	[48]
<i>Pseudomonas aeruginosa</i>	Bacteria	82%	[49]
<i>Pseudomonas putida</i>	Bacteria	69%	[50]
<i>Aeromonas hydrophila</i>	Bacteria	40%	[51]
1-4 <i>Comamonas testosteroni</i>	Bacteria	40%	[51]
1-4 <i>P. plecoglossicida</i>	Bacteria	34%	[51]
<i>Corynebacterium glutamicum</i>	Bacteria	34%	[52]
<i>P. monteilli</i>	Bacteria	47%	[51]
<i>Lysinibacillus fusiformis</i>	Bacteria	25%	[51]

3.1. Advanced Oxidation Process (AOP)

Advanced oxidation processes (AOPs) were first proposed in the 1980s for the treatment of drinking water and were later on widely used for the treatment of all kinds of wastewaters. The “advanced oxidation process” (AOP) can be used to degrade a large number of organic/inorganic pollutants by producing a range of strong hydroxyl radicals [53–55]. Basically, AOPs are based on the generation of strong oxidants in situ, i.e., hydroxyl radicals and sulfate radicals, for the oxidation of a wide range of environmental pollutants. To make hydroxyl radicals, these approaches require a high-energy light source and an oxidant [56]. AOP has been touted as a viable solution for the treatment of organic chemical contaminants in wastewater, including dyes and pigments [57]. UV/H₂O₂ and UV/reagent Fenton’s AOP procedures are substitutes for the breakdown of organics in wastewater [58]. However, AOPs continue to be hampered by high costs and insufficient degradation. Photocatalysis, Fenton-like processes, and ozonation are the different types of AOPs. Photocatalysis is one of the advanced oxidation technologies which requires no oxidants (atmospheric oxygen) and utilizes natural sunlight of the reaction to initiate, uses an efficient semiconductor under UV/visible light irradiation, and does not require extra chemicals, is likely one of the most effective and cost-effective AOPs [59].

3.2. Photocatalysis and Basic Principle of Photocatalysis

To date, a variety of ways for removing colors from water have been proposed, including chemical and biological methods; they can no longer be used because of their high cost, slow process, toxicity, high power consumption, and creation of harmful by-products. Advanced oxidation processes, such as photocatalysis, appear to be an appropriate approach for dye degradation to overcome the constraints of conventional technologies [60]. Heterogeneous photocatalysis is a well-known AOPs and alternate technique for the treatment of dye effluent among AOPs; because photocatalysis is highly prospective, active, and lowers energy consumption, it could be an effective method for removing dye contaminants [61,62]. The fundamental benefit of photocatalytic degradation is that it eliminates the need for waste disposal because harmful contaminants are broken down into carbon dioxide, water, acid, and other simple salts [63].

Photocatalysis is defined as a change in the rate of chemical reactions or the beginning of chemical reactions in the presence of light within the sight of a photocatalyst [64]. They are a type of combination that, when exposed to light, produces an electron-hole pair and causes chemical reactions in reaction substrates that come into contact with them. They then go through the process of recovering their distinctive electrical composition. Different organic contaminants can be eliminated photocatalytically under the influence of an effective light source such as UV or solar light, as has been demonstrated several times. The oxidation interaction in photocatalysis has earned it a reputation for the capability of producing hydroxyl radicals [65]. One of the most important advanced oxidation technologies is photocatalysis. It is commonly used for both oxidative and reductive wastewater treatment, such as the reductive deposition of metals from wastewater.

It is critical to select the best photocatalyst possible. The following characteristics should be present in a perfect photocatalyst:

- Chemical and photonic stability;
- Ability to absorb reactants under adequate photonic activation;
- Acquire a bandgap where the hydroxyl radicals’ oxidation potential and the superoxide radical’s reduction potential are within the gap;
- Availability is simple.

The bandgap plays a crucial role in photocatalytic degradation. Modification of nanomaterials lowers the bandgap and enhances photocatalytic efficiency.

3.2.1. Mechanism of Photocatalysis

The photocatalysis method is based on the activity of a semiconductor under irradiation light, such as solar or ultraviolet light, which can generate charges [66]. When

photons with sufficient energy penetrate a semiconductor, an electron may be ejected from its valance band energy level and into the conduction band, leaving a hole (h^+) [67]. An electron-pair generation is a term used to describe this occurrence. In the presence of a continuous energy supply, these electron pairs are consistently created [68]. The oxidized organic molecules are formed as end products in indiscriminating degradation at the photocatalyst surface via similar and sequential redox reactions. Figure 2 shows a schematic representation of the mechanism of oxidative species liberation from a photocatalytic study for dye degradation.

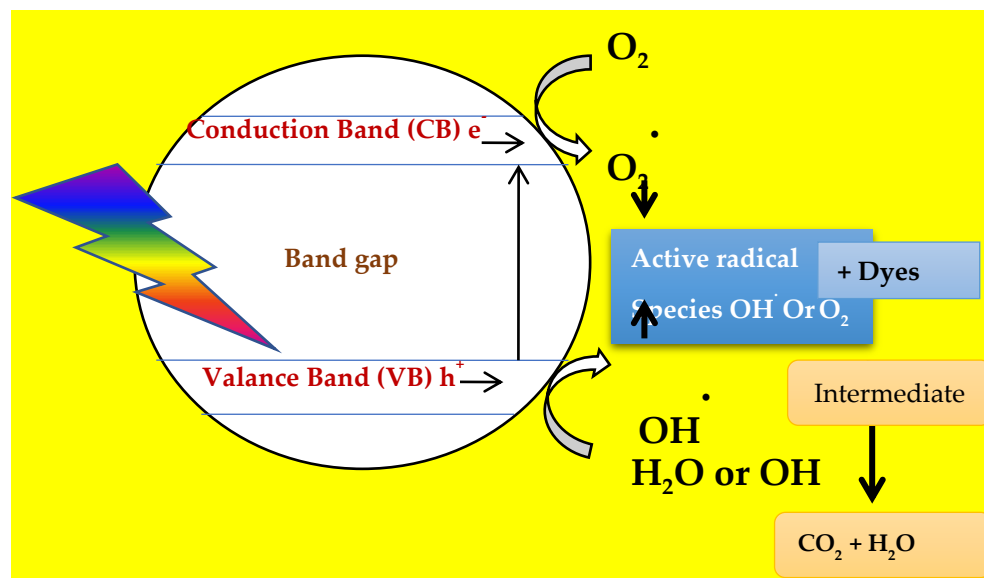
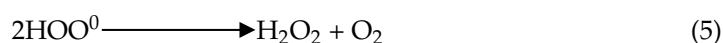
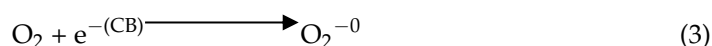
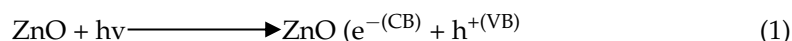


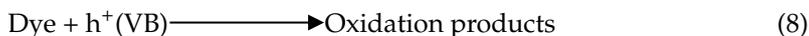
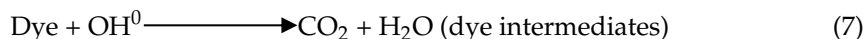
Figure 2. Mechanism for photocatalytic degradation.

The general mechanism is presented, and subsidiary steps might be added based on the experimental conditions. This approach is regarded as the most successful since it results in the near-complete mineralization of diverse chemical compounds. Aside from that, the adoption of low-cost semiconductors amplified the significance of this technique [69]. In general, a heterogeneous catalytic reaction necessitates five steps [70]:

- Adsorption onto the surface;
- Reaction on the surface;
- Desorption of products from the surface;
- Diffusion of reactant molecules from the bulk to the surface;
- Product diffusion to the masses.

The superoxide (O_2^{-0}) produced becomes protonated to form hydroperoxyl radical (HO_2^0) and then subsequently H_2O_2 , which further dissociates into highly reactive hydroxyl radicals (OH^0). The resulting OH radical, being a very strong oxidizing agent (standard redox potential + 2.8 V) can oxidize most of the MB dye; the mineral end-product substrates not reactive toward hydroxyl radicals are degraded employing ZnO photocatalysis with rates of decay and are highly influenced by the semiconductor valance band edge position [71].





The degradation of different dyes is caused by the excited electron and hole in the semiconductor. A wide range of semiconductors has been used, with the vast majority of them being used in the nano-state because of their increased surface area and high quantum size impact. Furthermore, the processes can be carried out at room temperature and normal pressure. Furthermore, this technique can use sunlight as a sustainable, high-access, and low-cost light source (depending on the semiconductor type and band gap), which is less expensive than alternative procedures that require ozone formation, electrodes, or other expensive components [72].

There are several studies where MB has been reported to be degraded by zinc oxide or zinc oxide nanoparticles. One such study was carried out by Balcha et al. (2016) where ZnONPs of size 28–30 nm synthesized by sol-gel was used for the photocatalytic degradation of MB dye up to an efficiency of 92.5%. The remediation of MB dye by photocatalytic ZnONPs/NiFe₂O₄ is shown below in the schematic diagram, Figure 3, as reported by Adeleke et al. (2018) [73].

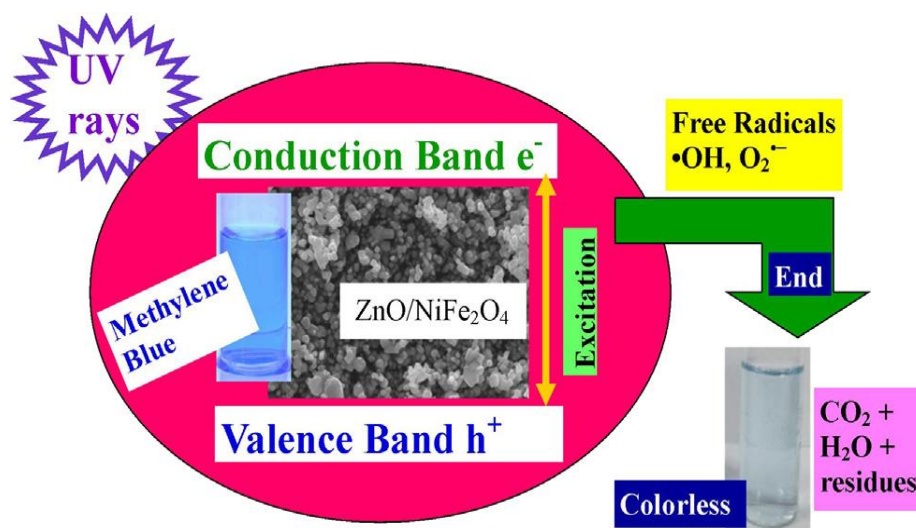


Figure 3. Photocatalytic degradation of MB dye by ZnONPs/NiFe₂O₄ "Reproduced with permission from [Adeleke et al. (2018)], [Applied surface science]; published by [Elsevier, 2018]. [73] (License NO is 5312450835938).

Houas et al. (2001) also reported the effect of various factors on MB dye removal. The author showed the disappearance of MB dye by photolysis and photochemistry under UV light at different wavelengths, as shown in Figure 4 [74].

3.2.2. Photocatalysis Reaction Kinetics

The kinetics and mechanism of photocatalysis are largely determined by experimental parameters, such as pH, temperature, catalyst dose and type, dissolved oxygen concentration, presence of an oxidant, substrate concentration, concentration of intermediates produced, and presence of inorganic ions [75]. To explain heterogeneous catalysis, the Langmuir Hinshelwood kinetics model (L-H) is commonly utilized. The photocatalytic rate[®] is proportional to the organic substrate's surface covering fraction,

$$r = \frac{K_a k_r C}{1 + K_a C} \quad (10)$$

where r is the reactant's oxidation rate ($\text{mgL}^{-1}\text{min}$), C is the reactant's concentration (mg L^{-1}), t is the irradiation period, k_r is the reaction's rate constant ($\text{mgL}^{-1}\text{min}$), and K_a is the reactant's equilibrium constant on the catalyst surface (Lmg^{-1}).

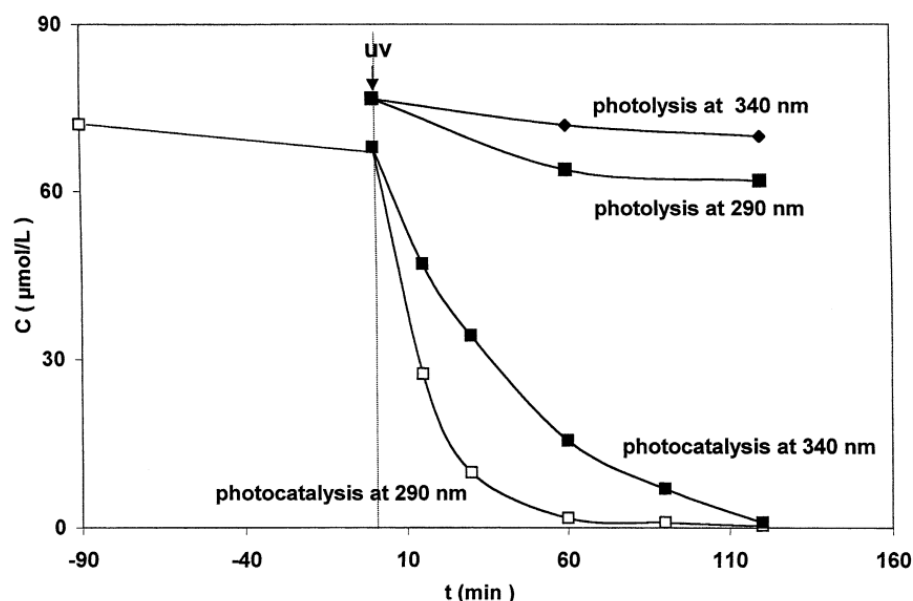


Figure 4. Remediation of MB dye by photochemistry and photocatalysis by UV irradiation at 290 and 240 nm, adopted from Houas et al. (2001) [74].

At lower substrate concentrations, the photocatalytic degradation of organic molecules follows pseudo-first-order reaction kinetics. The relationship between reactant concentrations at time t is represented by the equation below. Taking the equation and integrating it,

$$\ln \frac{C_0}{C} + (C_0 - C) = k_r K_a t \quad (11)$$

The equation can be simplified to a first-order equation in the form:

$$\ln \left(\frac{C_0}{C} \right) + k_r (C_0 - C) = k_r K_a t \quad (12)$$

where C_0 is the initial concentration of the pollutant in solution, and C is the residual concentration of the pollutant [76].

4. Zinc Oxide as Photocatalyst

Heterogeneous photocatalysts are solids that can promote catalytic reactions in the presence of light without being consumed in the process [77]. TiO_2 , ZnO , SnO_2 , ZrO_2 , SiO_2 , WO_3 , CeO_2 , and other semiconductor materials are employed in photocatalytic reactions and can be used as photocatalysts because of their capacity to decolorize dye-containing wastewater [78,79]. Out of all of them, ZnO emerges as one of the best photocatalysts due to its unique physicochemical properties.

Zinc oxide (ZnO) is an II-IV semiconductor with a wide direct band gap of 3.37 eV and a large exciton binding energy of about 60 mV at 300 K [80]. ZnO typically appears as a white-colored powder. It has near insolubility in water. It is also optically transparent under the visible range. ZnO can be crystallized in three forms under different conditions: hexagonal wurtzite, cubic zinc blend, and rock salt structure [81]. Among all three structures, the hexagonal wurtzite structure of ZnO is the most thermodynamically stable. Under ambient conditions, ZnO crystallizes into the wurtzite structure with great preference [82]. Due to its properties, lower cost than other catalysts, easy availability, ZnO has been one of the most popular choices of the photocatalyst. It also possesses excellent quantum efficiency

and solar absorption capacity, which lead to higher photocatalytic activity [83]. Compared to TiO₂, ZnO nanoparticles have a large surface-area-to-volume ratio, high UV absorption capacity and long life span [84].

The most common chemical methods for ZnO NPs synthesis are chemical reduction, microemulsion (colloidal) techniques, sonochemical reduction, electro-chemical, hydrothermal, and microwave-assisted methods [85]. Surfactant- or polymer-based preparative methods for nanoparticles synthesis are also a quite popular approach to avoid agglomeration and controlled synthesis of nanoparticles [86]. The homogeneous chemical precipitation method is considered economically viable for the synthesis of monodisperse metal oxide particles of different sizes and shapes. The method also provides better control of morphological and chemical characteristics [87].

Ghorbani (2015) synthesized ZnO nanoparticles by the precipitation method using zinc nitrate as a precursor and potassium hydroxide as a precipitating agent in an aqueous solution. ZnO nanoparticles were characterized by UV visible spectroscopy, transmission electron microscopy (TEM) and dynamic light scattering (DLS) techniques. The size range of synthesized ZnO powder was approximately 20–40 nm.

The least possible number of chemicals is utilized during the biological route for the synthesis of nanoparticles that produce the least amounts of pollutants. So biological approaches for nanoparticle synthesis using plants and microorganisms have been suggested as safe and eco-friendly alternatives to chemical methods. Bacteria can reduce metal ions and show the ability to precipitate at a nanometer scale [88]. Several natural moieties, such as plants, bacteria, fungi, algae and viruses, are used for ZnO synthesis [89].

Recently, there has been a growing necessity to develop eco-friendly methods that do not use any toxic materials during the synthesis process. To date, a number of physical, chemical and biological methods are available for the synthesis of different nanomaterials. The synthesis of nanoparticles by using different parts of plants is novel, which leads to truly green chemistry, as it is reduced or no need for energy, high pressure, temperature, and toxic chemicals. Moreover, it is effective at a very affordable cost [90]. The use of algae for the synthesis of nanoparticles has become prevalent these days due to their high efficiency and easy access. The biomolecules present in algae or algal extract have relatively been exploited for the synthesis of nanoparticles than other biological resources, such as bacteria and plants [91]. The perspective of developing new materials by combining biological and inorganic components has caused rising interest in many scientific groups [92].

Anbuvaran (2015) employed a biological technique to generate ZnO NPs for dye degradation. They reported the synthesis of ZnO NPs, by using *Phyllanthus niruri* leaf extract as a reducing agent. The ultra visible-differential reflectance spectroscopy (UV-DRS), photoluminescence (PL), X-ray diffraction (XRD), Fourier transform-infrared spectroscopy (FTIR), field emission scanning electron microscope (FE-SEM), and transmission scanning electron microscope (TEM) methods were used to characterize the produced nanoparticles. The obtained results confirmed the estimated bandgap of 3.51 eV at 402 nm and PL intensity [93].

5. Dye Removal: Bioremediation to Nanoremediation

Because of its simplicity and lower cost, dye biodegradation via traditional two-stage aerobic/anaerobic activated sludge or immobilized biofilm processes is the most widely used method worldwide [94].

Contreras et al. (2012) used *Galactomyces geotrichum* KL20A, a Kumis isolate, to remove MB dye. The initial dye concentration and growth temperature were tested at three different levels in the bioremediation process. The duration of the exposure was 48 h. Under the best-operating conditions, clearance percentages of MB dye were found to be greater than 70%. The researchers also carried out a cytotoxicity investigation. When compared to the hemolytic activity of the negative control, the by-products recovered following the bioremoval procedure had a substantially lower proportion of hemolysis (22%) than the

negative control (100 %). Their findings indicate that the isolated strain is capable of removing large levels of MB from wastewater effluents [95].

The bioremediation of dye chemicals utilizing indigenous microorganisms was reported by Bhawana and Fulekar (2012). They used physicochemical and microbiological studies to analyze the dye effluent collected in their investigation. Microbes from the wastewater were identified and cultivated for use as biomass in bioremediation. GC-MS analysis revealed the presence of organic chemicals. The consortium was used to bioremediate dyestuff in a laboratory-scale bioreactor over a 21-day timeframe. GC-MS analysis was used to track the biodegradation of organic components in industrial wastewater at regular intervals until the biodegradation was complete. The intermediate chemicals generated during the process were degraded to phthalic acid, a non-toxic substance. Their findings revealed that the dye chemicals were effectively degraded by an indigenous microbial community into environmentally favorable products [96,97].

Eslami et al. (2017) tested the biodegradation of MB dye from an aqueous solution by bacteria isolated from contaminated soil on a laboratory scale. The dominating bacteria was found to be *Pseudomonas aeruginosa*. Researchers found that increasing the initial MB concentration from 50 to 200 ppm increased the clearance effectiveness of germs from 82.25 to 97.82 %. The clearance effectiveness was lowered to 43.08 % when the MB concentration was increased from 200 to 1000 ppm. The findings revealed that the bacteria utilized MB as a carbon source in addition to glucose. *P. aeruginosa* was shown to be an effective alternative for removing MB from the environment by researchers [98].

Chavan and Fulekar (2018) described a new technique to increase the degradation efficiency of CETP wastewater using integrated treatment processes, such as photocatalytic oxidation and biodegradation. During their research, they used a hybrid photocatalyst impregnated with activated carbon for photocatalytic oxidation and a created biofilm on a biocarrier for biodegradation. In the presence of solar light, TiO₂/activated carbon, and biofilm, the percent degradation efficiency of chemical oxygen demand (COD), biological oxygen demand (BOD), total suspended solids (TSS), and NH₃-N during 6 h were 61 %, 92 %, 88 %, and 50 %, respectively, and color removal was 78 %. Their findings showed that using an impregnated TiO₂/AC photocatalyst provides a high surface area and photocatalytic rate in photocatalytic oxidation, which generates radicals in the presence of sunlight, attacks toxic pollutants, and converts them to biodegradable pollutants, which are then mineralized by biofilms [99].

Nanoparticles offer a lot of potential for wastewater treatment because of their unique properties. Bio-nanotechnological solutions have recently proven to be crucial in avoiding the problems related to dye-bearing wastewaters. The emergence of biomimetic nanotechnology sparked the concept of combining bioremediation and nanotechnology to create a revolutionary technology. Nanobiotechnology is the name given to the confluence of these two existent technologies. The use of nanomaterials in conjunction with living bacteria is known as nanobiotechnology [100].

Enzyme-assisted wastewater treatment is effective for refractory contaminants and requires only mild reaction conditions, making it environmentally friendly. Nanoparticles are utilized as a vehicle for a variety of enzymes that degrade contaminants found in textile effluent [101].

Aber et al. (2016) reported the synthesis of magnetite NPs and used them as support for glucose oxidase immobilization. A pH of 6, the temperature of 10 °C, glucose oxidase/support ratio of 1800 U/g, and time of 2.5 h were the optimal immobilization conditions. In these settings, 450 units of glucose oxidase/gram of magnetite were immobilized. In batch experiments, immobilized glucose oxidase was utilized to decolorize acid yellow 12. The researchers concluded that the dye removal efficiency of the magnetite immobilized enzyme was improved [102].

Carata et al. (2017) applied a nanobiotechnological approach to transforming pollutants in water, air, and soil into environmentally benign chemicals. The technique can be used to avoid water pollution, treat wastewater, remediate dangerous contaminants,

and produce contamination identification sensing and detection systems [103]. Although nanobioremediation is superior to traditional treatment approaches, there may be certain concerns associated with environmental nanotoxicity.

6. Treatment of Industrial Effluent Using ZnO Nanomaterials

The remediation of dye substance compounds has become a hot topic in recent years because of too stringent government legislation and environmental regulations. Textile dyes must be removed from colored industrial waste effluents to safeguard the environment and ensure long-term sustainability [104]. In terms of BOD, COD, color, salinity, suspended solids, and pH, effluent discharged in water bodies from dye manufacturing and textile industries has negative effects on the environment, demonstrating that these effluents contain a large proportion of nonbiodegradable organic matter that must be treated with new and modified techniques [54,105].

The potential applications of ZnO nanoparticles in the form of nano-sorbents, nano-sized plates, nano-composite film, and hybrid or doped nanoparticles for the treatment of industrial wastewater with heavy metal and color content were examined by Nagar and Pradeep (2020) [106]. According to researchers, ZnO NPs impregnated in the polymer matrix are not expelled with effluents. Nano-composites can be regenerated using 0.1 M HNO₃ or 0.1 M NaOH as a desorption agent. According to their research, the modified ZnO material can be used to replace high-cost artificial UV light with visible solar light.

Abul et al. (2015) employed a chitosan zinc oxide composite as an adsorbent for the removal of two colors from a textile industrial waste effluent sample: Reactive Black HN and Reactive Magenta HB. The color removal efficacy of chitosan ZnO NC was tested using such parameters as temperature, composite loading, contact time, and turbidity during their research. Color removal from a textile sector effluent was studied using batch adsorption, and 95–99 % efficiency was attained. It was discovered that by utilizing 2 gm of composite per liter of effluent at room temperature (50 °C) and 60 min of contact time, 99 % of the effluent's natural color could be removed. Researchers discovered that when the dose of composite and temperature rises, so does color adsorption [107].

Hairom et al. (2015) sought to remediate industrial dye effluent with ZnO NPs in a membrane photocatalytic reactor (MPR) [108]. The precipitation process was used to make ZnO NPs. Researchers discovered that pH 11 and 0.1 g/L ZnO loading were the MPR's optimal operating conditions. In the presence of ZnO-PVP-St as the photocatalyst in the MPR, the performance of the NF membrane and the chemical properties of the effluent were improved in terms of normalized flux reduction (65%), color removal (100%), COD reduction (92%), turbidity reduction (100%), and total suspended solid rejection (100 %). Due to the permeability of dye molecules and ZnO NPs over the UF membrane pores, the UF membrane performed poorly. The results show that the MPR system has greater promise in the treatment of industrial wastewater [108].

In the presence of ZnO-polyvinylpyrrolidone (PVP) nanoparticles (0.025 g/L of PVP), Sidik et al. (2018) proposed photocatalytic degradation of industrial dye effluent. During the precipitation type of ZnO synthesis, PVP was used as a capping agent. The chemical linkages in ZnO-PVP were studied using FTIR analysis. The rate of dye degradation was determined to be 90.61 percent in the presence of ZnO-PVP at pH 7. The photocatalytic degradation of industrial dye effluent by ZnO-PVP NPs offers significant potential as an alternative treatment, according to researchers. It is an environmentally friendly treatment because no toxic by-products are produced [109,110].

Blazeka et al. (2020) synthesized ZnO NPs using the laser ablation method, having an average size of about 47 nm for the photocatalytic degradation of methylene blue and Rhodamine B dye under UV light irradiation. The photocatalytic degradation efficiency is about 40% higher for methylene blue dye compared to Rhodamine B dye. It was reported that the photodegradation rate is much larger at lower dye concentrations; as the concentration of dyes increased, photocatalytic degradation was found to be decreased.

Mydeen et al. (2020) synthesized ZnO NPs using *Prosopis juliflora* leaf extract (ZLE) and citric acid (ZCA) for the photocatalytic degradation of MB dye and antibacterial activities. The energy band difference values are 3.23 and 3.25 eV, and ZLE NPs are blue-shifted, which is recognized as an influence of leaf extract, according to UV-DRS data. In the presence of ZnO NPs, the MB dye was found to be effectively destroyed under UV radiation. ZLE NPs degrade well within 45 min, according to researchers [111].

Under UV light irradiation, Balcha (2016) examined the photocatalytic degradation of methyl blue by ZnO NPs produced by precipitation and sol-gel methods. The hexagonal wurtzite structure of ZnO NPs generated by precipitation and sol-gel techniques was revealed by XRD data, with crystallite sizes of 30 and 28 nm, respectively. The effects of operational parameters, including the starting dye concentration and photocatalyst load were looked at. The photocatalytic degradation process follows the pseudo-first-order reaction, according to researchers. They found that ZnO NPs made by the sol-gel approach had higher photocatalytic activity than those made by the precipitation method [112].

Delaying electron-hole recombination, broadening the absorption spectrum, facilitating particular specific processes on the surface of photocatalysts [113], and improving photo-stability are all advantages of photocatalyst modifications. Doping transition metals such as Ag, Pd, Pt, Au, Sn, In, and Fe with ZnO proved effective in overcoming the difficulties of anodic photo-corrosion and instability of ZnO in acidic or alkaline conditions [114,115].

Nanostructured ZnO has received a lot of attention in recent years because of its unique properties and novel applications in optoelectronics, optics, pyroelectricity, piezoelectricity, and catalysis [116,117]. Because of its unique benefits, such as lower price, strong photocatalytic activity, and non-toxicity, the degradation of pollutants catalyzed by ZnO has been extensively explored [118]. The catalyst's main drawback is that its catalytic activity is currently insufficient for commercial use [119] and has also shown toxicity due to its nanosize. Several investigators have reported the toxicity of ZnONPs due to their small size, for instance, Liu et al. (2017), Vandebriel and De Jong (2012) and Sruthi et al. (2018). Doping is performed by adding some hetero-elements to boost the photocatalytic property efficiently and practically. The photocatalytic activity, charge carrier recombination, and interfacial electron-transfer rate is all affected by the presence of doping material in the ZnO crystalline matrix [120]. Transition metal ions, such as Co^{2+} , Mn^{2+} , Mn^{4+} , Ti^{4+} , La^{3+} , Fe^{3+} , and so on, are commonly used [121,122].

Zhang and Zeng (2012) used a typical sol-gel procedure to try to make a Cd-doped ZnO photocatalyst for the degradation of MB dye under visible light irradiation [123]. The effects of essential operational parameters, such as beginning dye concentration, catalyst loading, and initial pH value on decolorization extents, were investigated. According to the obtained data, the decolorization of organic molecules followed pseudo-first-order kinetics according to the Langmuir–Hinshelwood model. Under optimal conditions, roughly 85 percent of the color may be removed in 3.5 h [123].

Omidi (2013) employed ultrasonic irradiation to generate Sb-doped ZnO nanostructures for the photodegradation of MB dye. The nanostructures that were generated were characterized using XRD, SEM, FTIR, and UV-DRS. The observed results demonstrated morphological and size variations in doped nanostructures when compared to pure ZnO. Doping ZnO nanostructures with 0.03 Mol% Sb^{+3} ions triple the reaction rate, which the researchers attribute to decreased charge carrier recombination. At pH 5.4, they discovered that doped nanostructures with a concentration of 0.4 g/L exhibited the highest photocatalytic activity [124].

Shirini (2015) synthesized tungsten (W) doped ZnO nanocomposite and further analyzed it by using XRD, TEM, BET, SEM, and ICP-OES. The nanocatalyst created was then used to synthesize biscoumarins in water. The surface area of W-ZnO ($93.70 \text{ m}^2/\text{g}$) was quite considerable. The TEM images show very small particles, less than 20 nm in diameter. According to ICP-OES data, the weight ratio of W/Zn in W-ZnO nanocomposite was 0.228% [125].

When exposed to UV radiation, Sanoop (2016) generated yttrium (Yt) doped ZnO to eliminate the MB dye. In terms of photocatalytic activity, researchers discovered that doped nanoparticles outperformed pure ZnO. The kinetics of the photodegradation reaction carried over MB dyes exhibited first-order reaction kinetics for ZnO samples containing 1 mol% Y_2O_3 . When the Y_2O_3 doping level was greater than 5 mol%, the catalytic reaction displayed second-order reaction kinetics. At pH 10, all of the samples included in the study had maximum photocatalyst efficiency. According to the reusability tests, Yt doping improved the stability of the ZnO samples [126].

Hemalatha et al. (2016) created lanthanum (La) doped ZnO flower-like nanoparticles, using a microwave-assisted sol-gel technique. XRD measurements indicated the effective incorporation of the lanthanum ion into the ZnO lattice. Short-duration UV light irradiation of 20 mg/L of MB interacting with 90 mg/150 mL of 3 mol percent La-doped ZnO nanorods resulted in maximum MB dye degradation of up to 95 % (60 min). Several operational parameters, such as dye concentration, photocatalyst quantity, and dopant concentration, were optimized during the investigation [127].

Bhatia (2016) used a simple combustion approach to quickly produce Er-doped ZnO NPs for photocatalytic degradation of direct red-31 dye [128]. During the investigation, several concentrations of Er 2.0 at. wt%, 2.5 at. wt%, 3.0 at. wt %, and 3.5 at. wt % were used as dopants. The concentration of Er as a dopant was found to have a significant impact on the band gap, morphology, and photocatalytic efficacy of ZnO NPs. The photocatalytic tests revealed that the degradation percentage increased with increasing the Er concentration up to 2.5 at. wt. %, which showed nearly complete degradation in only 60 min when exposed to UV light. All samples, according to kinetic studies, follow the first-order rate constant [128,129].

Zandsalimi et al. (2018) reported the synthesis of tungsten-doped ZnO by the hydrothermal method. During the study, tungsten oxide was injected into the structure of ZnO at concentrations of 0.5, 1.0, and 2.0 % and analyzed using SEM, XRD, FTIR, DLS, atomic force microscope (AFM), and UV-Vis spectroscopy. SEM and XRD measurements corroborated the hexagonal and non-aggregated structures of ZnO and doped-ZnO nanostructures. According to DLS data, doping was found to diminish the particle size of ZnO. According to UV spectra and AFM tests, the doping of ZnO nanostructures caused a spectrum change in the absorbance of ZnO from ultraviolet to the visible area, increasing their relative roughness [130].

Vallejo et al. (2020) reported the synthesis and characterization of Ag-doped ZnO thin films by employing the sol-gel method. The doctor blade technique was used to create the thin films. The samples were polycrystalline, and the diffraction signals corresponded to the ZnO wurtzite crystalline phase, according to the physicochemical characterization data. Under visible light irradiation in the aqueous phase, Ag-doped ZnO thin films were employed for the photocatalyst breakdown of MB dye. The presence of Ag improved the optical properties of ZnO in the visible region, according to the optical data, and the Ag-doped ZnO thin films exhibited the lowest band gap value (2.95 eV). The method improved the photocatalytic response under visible light irradiation, according to the researchers, and the Ag-doped ZnO thin films exhibited the greatest MB photodegradation value (45.1%) when compared to the ZnO thin films (2.7 %) [131].

6.1. Co-Doped ZnO for Removal of Dye

Vignesh et al. (2014) used the co-precipitation approach to make Nickel (Ni) and Thorium (Th) co-doped ZnO NPs. The degradation of MB dye under visible light irradiation was used to assess the photocatalytic activity of the produced co-doped ZnO. Ni-Th-ZnO exhibits a hexagonal and rod-like shape, with an average crystalline size of 30 nm, according to XRD and SEM data. The greatest MB degradation (93 percent with 70% COD elimination) was reached with a Ni-Th-ZnO concentration of 0.375 g/L, an initial MB concentration of 1.5 M, pH 10, and an irradiation period of 180 min, according to the researchers. A

photocatalytic mechanism was proposed as well. The photocatalyst could be utilized four times without losing its activity significantly [132].

6.2. ZnO Nanocomposites for Removal of MB Dye

The term “nanocomposite material” [133] has broadened greatly over the years to include a wide range of systems, including one-dimensional, two-dimensional, three-dimensional, and amorphous materials, which are made up of distinctly diverse components and blended at the nanoscale scale [134]. “Materials having a nanoscale structure that improves the macroscopic qualities of products” are nanocomposites. Clay, carbon, or polymer nanocomposites, or a mixture of these materials with nanoparticles as building blocks, are used. When compared to their bulk-sized counterparts, they have an exceptionally high surface-to-volume ratio, which dramatically affects their properties. Nanocomposite materials can be 1000 times more durable than bulk component materials. Nanocomposites have the potential to significantly improve qualities, as shown in [135].

For the photodegradation of MB dye under visible light irradiation, Prihashemi and Yangieh (2013) synthesized an AgBr-ZnO nanocomposite in water by refluxing about 90 °C for 3 h. XRD, SEM, EDX, UV-Vis DRS, and FTIR methods were used to examine the produced nanocomposites. According to the XRD results, AgBr loading does not affect the wurtzite hexagonal crystalline phase of ZnO. The SEM image shows that the surface morphology of the samples changes to nanorods with lower diameters as the mole fraction of AgBr increases. The nanocomposites were discovered to have more activity than pure ZnO and AgBr during the research. Furthermore, the impact of several operating parameters on degradation was investigated. Under visible light irradiation, chemical oxygen demand (COD) measurements were used to check the mineralization of MB on the nanocomposite [136].

Ma et al. (2014) used a simple one-step photochemical approach to synthesize ZnO/Ag₂O heterostructures for the elimination of MB dye in deionized water, Changjiang River water, and tap water with great efficiency under UV and visible light irradiation. When compared to pure ZnO and Ag₂O, the UV and visible photocatalytic activity of the produced ZnO/Ag₂O heterostructures was dramatically increased. The deterioration rates of ZnO/Ag₂O heterostructures were 27.4 and 15.6 times quicker than those of bare ZnO, respectively. Aside from that, due to the lower concentration of surface imperfections, the produced ZnO/Ag₂O heterostructures could be easily recycled in UV and visible photocatalytic applications [71].

Saravanan (2014) used a simple thermal decomposition approach to make a vanadium pentoxide (V₂O₅)/ZnO nanocomposite for the photocatalytic degradation of MB dye under visible light irradiation. Because of its narrow band gap, V₂O₅ has attracted a lot of attention as a potential visible light catalyst for the degradation of organic contaminants. Nonetheless, the rapid recombination of electron-hole pairs limits the use of V₂O₅ in pollutant photodegradation. Researchers have combined V₂O₅ with other semiconductors, such as ZnO, to overcome this constraint. XRD examination revealed the production of orthorhombic-structured V₂O₅ and hexagonal-structured ZnO. The nanorod production of produced composites was revealed by HR-SEM data. The nanocomposites are made up entirely of vanadium, zinc, and oxygen, as determined by electron diffraction analysis (EDX) [137].

The effect of granular activated carbon (AC) coated with ZnO NPs (AC-ZnO) on the removal of MB and Acid orange 7 dye from an aqueous solution was examined by Nourmoradi et al. (2015). The shape of AC and AC-ZnO was determined using SEM, and the significant interaction between AC and ZnO was validated using FTIR spectra. In comparison to raw AC, the Langmuir isotherm and pseudo-second-order kinetic models fit the experimental data better, while AC-ZnO was more efficient [138].

Nasir (2016) used the sol-gel process to create a unique TiO₂-ZnO-CoO nanocomposite for the photodegradation of MB dye. TiO₂ and ZnO are photocatalysts for the photodegradation of organic contaminants in general. The disadvantages and limitations of TiO₂ and

ZnO's photocatalytic activity occur largely in the UV range and less in visible light. The goal of this work was to use cobalt oxide to reduce the disadvantages of TiO₂ and ZnO. The mass ratio of O: Ti:Co: Zn in TiO₂-ZnO-CoO nanocomposite was 32.64:37.39:11.85:18.12, according to the EDS analysis. The best photodegradation condition for MB was found to be pH 7, with a degree of degradation of 36.98 % for 60 min [139].

For the sonocatalytic decolorization of MB dye, Soltani et al. (2016) used a porous clay-like biosilica substrate for the production and immobilization of ZnO nanostructures. The ZnO-biosilica nanocomposite had a higher sonocatalytic activity (77.8%) than pure ZnO nanostructures (53.6 %). It was discovered that changing the initial pH from 3 to 10 resulted in a 41.8 to 88.2 percent increase in color removal. Increases in nanocomposite dosage from 0.5 to 2.5 g/L led to greater color removal, while increases up to 3 g/L resulted in a noticeable decline in color removal. The temperature-dependent sonocatalytic activity of ZnO-biosilica was also discovered. Within three consecutive experimental runs, the color removal (percent) in the reusability test research dropped by 15%. The ZnO-biosilica nanocomposite was found to be more efficient than pure ZnO NPs at absorbing the light irradiation created during cavitation, resulting in larger concentrations of OH radicals for dye molecule destruction [140].

Prasanna and Rajagopalan (2016) devised and synthesized a novel nanocomposite ZnO₂/polypyrrole that releases reactive oxygen species (ROS) in dark and light for MB dye and Rhodamine B degradation [141]. According to the researchers, the synergistically coupled nanocomposite of ZnO₂/polypyrrole is the first example of an improved oxidation process that destroys dyes in the dark without the use of extra chemicals. It should be emphasized that in the presence or absence of visible light, neither ZnO₂ nor polypyrrole could degrade these pigments. The nanocomposite's physicochemical synergy between ZnO₂ and polypyrrole makes it efficient for dye degradation [141].

Patil et al. (2017) reported the development of ZnO-bentonite nanocomposite for the photocatalytic degradation of MB dye. The accelerated oxidation process, according to researchers, is responsible for the breakdown of MB. The effects of initial dye concentration, pH, photocatalyst dose, and contact time on photocatalytic degradation were investigated. At pH 8, the maximum MB degradation was discovered after 80 min. Adsorption follows pseudo-second-order kinetics, according to the kinetic study. The adsorption isotherm was discovered to be similar to the Langmuir isotherm; a 62.5 mg/g monolayer coverage capacity was discovered. For a 0.2 g/L photocatalyst dosage at 60 mg/L MB concentration, the amount of dye adsorbed was found to be 252.7 mg/g [142].

Hosseini and Babaei (2017) studied the photocatalytic degradation of methylene blue dye using graphene oxide/zinc oxide (GO/ZnO) nanocomposite, ZnO NPs, GO, carbon nanotubes (CNT), and CNY/ZnO nanocomposite in comparison. The BBD of the response surface methodology effectively generated a second-order model for the photocatalytic process and forecasted the process (RSM). The photocatalyst dosage of 2.0 g/L, initial pH of 4.5, hydrogen peroxide (H₂O₂) concentration of 3.5 10⁻⁴ mol L⁻¹, and irradiation time of 140 min were found to be the best conditions for the removal of MB. Based on the Pareto analysis, the most effective factors were identified to be the irradiation period and photocatalyst dosage. According to the researchers, GO/ZnO could be a promising photocatalyst for dye cleanup [143].

Wang (2018) created a rectorite-based magnetic zinc oxide nanocomposite (REC/Fe₃O₄/ZnO) nanocomposite for MB dye adsorption and photocatalytic degradation. The ZnO component in the nanocomposite considerably aided dye degradation, with REC/Fe₃O₄/ZnO activity decreasing as the ZnO content increased. The dye on the composite adsorption isotherm fit the Langmuir model well, with maximum adsorption of 35.1 mg/g. The high adsorption capacity of the dye improved the contact between it and the REC/Fe₃O₄/ZnO nanocomposite, allowing for effective dye breakdown under simulated solar radiation. At pH 6.0, the maximum photoactivity for dye degradation was discovered. After three cycles, the mass loss and photoactivity of the produced nanocomposite only slightly decreased. During the research, the MB dye degradation route was also proposed [144].

Adeleke et al. (2018) reported the fabrication of a ZnO/NiFe₂O₄ nanocomposite for methylene blue dye degradation under UV and solar light irradiation. Both freshly synthesized ZnO and co-precipitated NiFe₂O₄ were calcined at a high temperature of 800 °C for 10 hours to generate the ZnO/NiFe₂O₄ nanocomposite. The results demonstrate that hydroxyl radicals and photo-produced holes are the major species involved in the removal of MB dye by generated nanocomposites. Here, the authors used a 50 mL solution of MB (at 500 mM), to which 20, 40, 50, and 75 mg of the ZnO/NiFe₂O₄ nanopowder was added. When compared to other concentrations of the same catalyst, the 75 mg ZnO/NiFe₂O₄ nanocomposite has the best photocatalytic activity [73].

The synthesized ZnONP was hexagonal in the shape of size 25 nm, while the NiFe₂O₄ was rod-shaped at 10–20 nm, as analyzed by the scanning electron microscope (SEM). In comparison to ZnO and NiFe₂O₄, the composite of both showed large agglomeration and different morphology. The SEM images of ZnO and NiFe₂O₄ and their composite are shown in Figure 5.

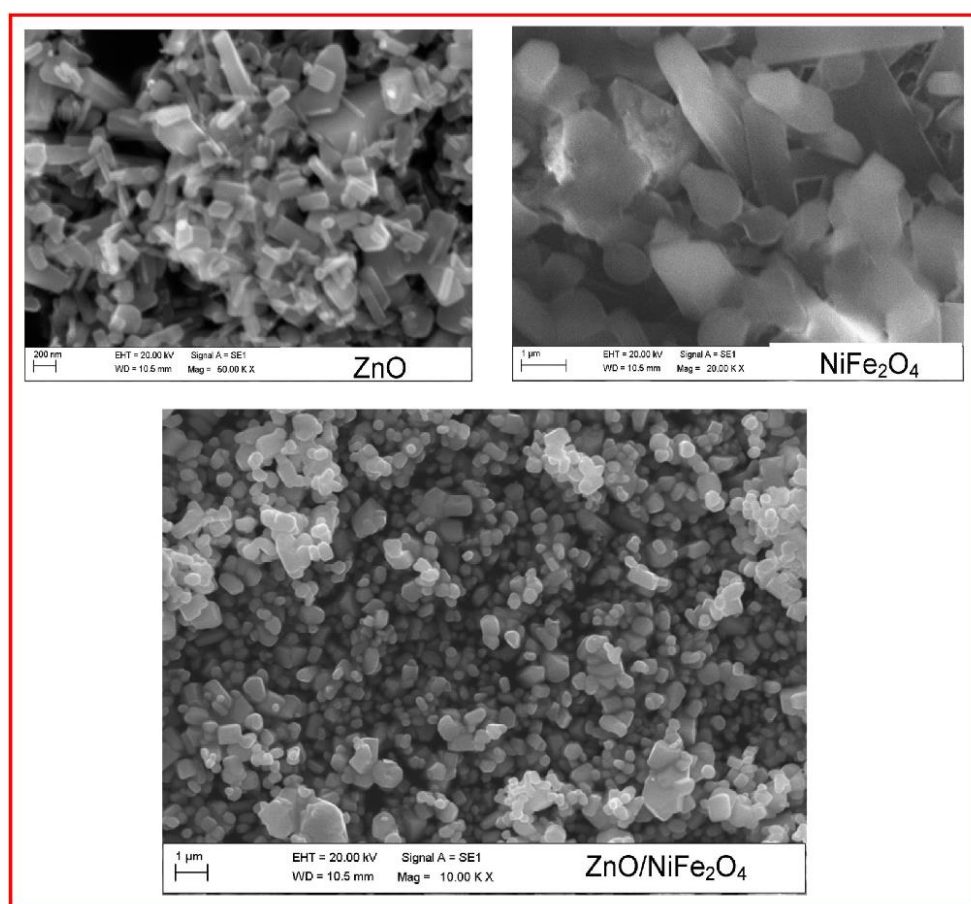


Figure 5. SEM micrographs of ZnO, NiFe₂O₄, and ZnO/NiFe₂O₄ were adopted from Adeleke et al. (2018) [73] (license no 5312450835938).

Figure 6 shows the absorbance spectra of MB dye by the varying concentration of nanocomposites, i.e., 50 mg and 75 mg for the removal of 50 mL MB dye from the aqueous solution. Figure 6 also shows the effect of time and irradiation time on the removal of MB dye from aqueous solutions.

Ritika et al. (2018) used a hydrothermal approach to make MoS₂-ZnO heterostructure nanorods for the photocatalytic degradation of MB dye using solar light. They discovered that the produced MoS₂/ZnO heterostructured nanorods removed 97 % of the MB dye in 20 min at pH 11 with a photocatalyst concentration of 0.15 g/L. The photocatalytic elimination of MB was found to follow pseudo-first-order kinetics, with a rate constant

of 0.162 min^{-1} , according to kinetic research. Scavenger studies and terephthalic acid fluorescence techniques were used to confirm the involvement of active species in the degradation of MB utilizing $\text{MoS}_2\text{-ZnO}$ heterostructure nanorods [145].

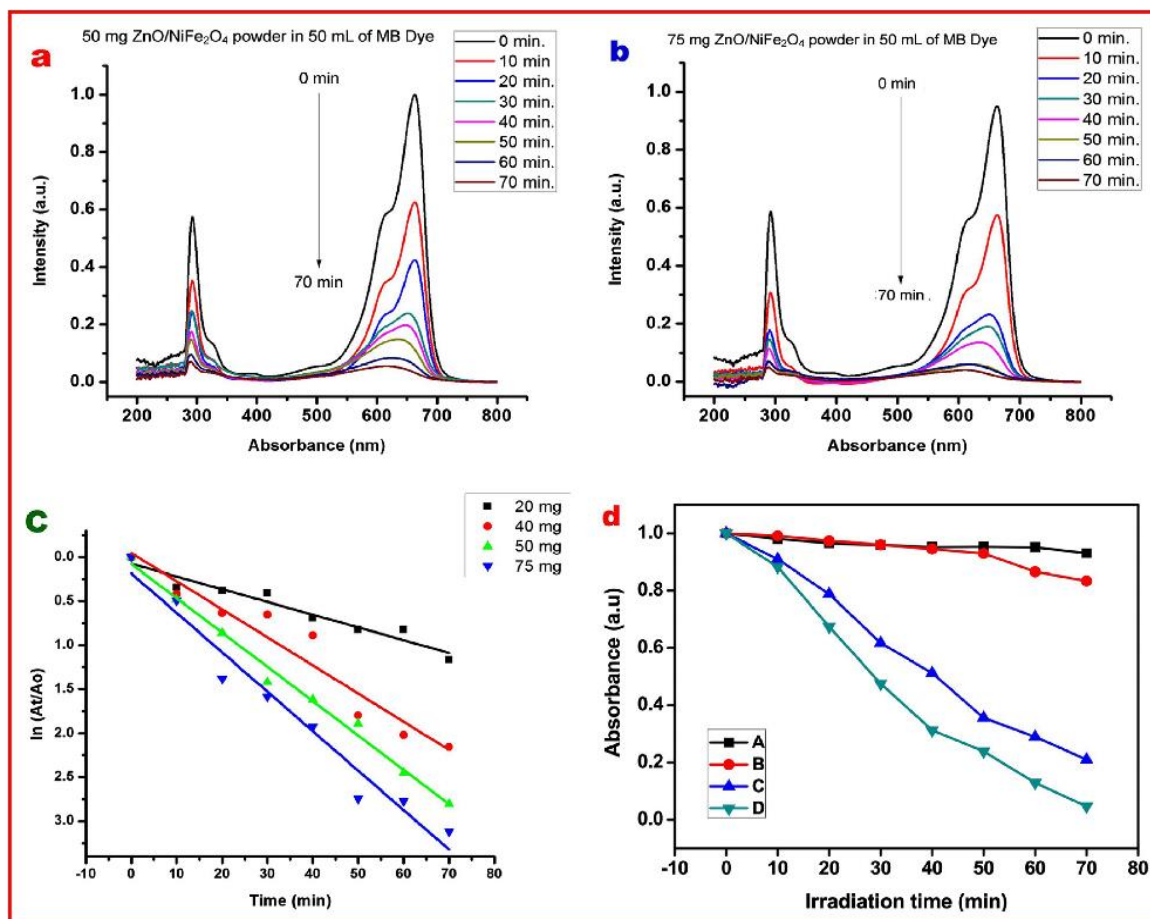


Figure 6. (a,b) Absorbance spectra of 50 mL methylene blue [$5 \times 10^{-5} \text{ M}$] dye solution containing 50 mg and 75 mg of $\text{ZnO/NiFe}_2\text{O}_4$ nano powder respectively. (c) The linear fitting for the absorbance spectra of MB dye solution containing 20 mg, 40 mg, 50 mg and 75 mg of $\text{ZnO/NiFe}_2\text{O}_4$ nano powder. (d) Photo-degradation and photocatalytic performances. (a) self-photo degradation of MB dye- with UV irradiation and absence of photo-catalysts. (b) MB dye and 75 mg of $\text{ZnO/NiFe}_2\text{O}_4$ absence of UV irradiation with stirring. (c) Bare ZnO 75 mg with MB dye. (D) $\text{ZnO/NiFe}_2\text{O}_4$ nano powder 75 mg with MB dye adopted from Adeleke et al. (2018) [73].

Munawaroh et al. (2018) presented their work employing graphene oxide (GO)/ZnO nanodrums to photocatalyze the breakdown of MB dye. During their research, they used the Hummer method to make GO and the hydrothermal approach to make ZnO. In distilled water, GO/ZnO nanodrums were mixed with varied compositions of GO and ZnO, such as 1:0, 1:1, and 1:2 (*w/w*). The degradation of MB by GO/ZnO nanodrums was reported to be 94.05 % after 60 min of contact time with UV exposure at 254 nm [146].

Micheal et al. (2020) used a wet chemical approach to manufacture rods such as ZnO nanoparticles and carbon nanoplates that supported ZnO nanorods (ZnO/C). Under visible light irradiation, the produced ZnO nanoparticles were employed to photodegrade the MB dye. When compared to pure ZnO, the ZnO/C photocatalyst showed excellent photocatalytic efficiency for the degradation of MB dye (95 %) within an 80 min irradiation time. Finally, for increased ZnO/C activity, the researchers presented a probable degradation route mechanism [147].

Lee (2015) used a spray-coating approach to create gold nanoparticles (Au NPs) that anchored graphene oxide (GO) on ZnO nanorods (Au/GO/ZnO) hybrids. The hybrid nanocomposite outperformed ZnO and GO/ZnO in terms of UV light absorption and photoluminescence emission quenching. When compared to ZnO and GO/ZnO, Au/GO/ZnO had the best photocatalytic activity for methylene blue dye degradation. For ZnO, GO/ZnO, and Au/GO/ZnO, the photodegradation efficiency of MB was found to be 62, 71, and 81 %, respectively. GC-MS analysis was used to look into the MB dye degradation mechanism [148]. Some reported research work for the removal of dye contamination using ZnO and ZnO-based nanomaterials (Modified ZnO) are listed in Table 2.

Table 2. Photocatalytic degradation of different dyes using ZnO and modified ZnO.

Type of Nanomaterial	Dye	Mode of Synthesis	Source of Light	Kinetics	Reference
ZnO	Acid red 14	-	UV light	First-order	[149]
	Eosin Y	Chemical	UV lamp	First-order	[150]
	Rhodamine B	Hydrothermal method	Solar light	First-order	[151]
	Acid Yellow 23	Chemical	UV light	First-order	[152]
	Acridine orange	-	Visible light	First-order	[153]
	Acid Blue 92	-	UV light	First-order	[154]
	Malachite green	Garcinia mangostana fruit pericarp extract	Solar light	First-order	[155]
	Congo red	Purchased from Merck	UV-A light	First-order	[156]
	Rhodamine B Acridine orange	Sol-gel methods	Solar light	-	[157]
	Alizarin Black S	Purchased from Alpha Chemika, India	UV light 254 nm	First-order	[158]
Direct red 23	Chemical synthesis	Low-pressure mercury lamp	First-order	[159]	
Methyl Red, Methyl Violet, MB Ethyl Eosin Safranin	Turnera subulata leaf extract	Solar light		[160]	
Modified ZnO (EDTA, Citric acid, Cis Oleic acid)	Malachite Green	Sol-gel	Visible light	First-order	[161]
Al-doped ZnO	Methyl orange	Chemical		First-order	[162]
Carbon black/ZnO NC	Methyl orange	Chemical-sonication	UV C light	First-order	[163]
BiOI/ZnO NC	Acid red 18	Chemical	Visible light halogen lamp (300W)	First-order	[164]
Chitosan ZnO NC	Congo red Brown BR	Chemical	Visible light		[165]

Based on the above studies, it was concluded that doping enhances the degradation ability of photocatalyst manifolds, and composites, and co-doping all aid in increasing the photocatalytic ability of nanomaterials, thus it is recommended to dope the photocatalyst with suitable dopants in order to enhance the efficiency of photocatalysis.

7. Conclusions

The present review focuses on the degradation of MB dyes using pure and modified ZnO. Photocatalytic degradation of dyes is a prospective and promising approach. Ac-

According to numerous literature and experiments, dye degradation mediated by ZnO and modified ZnO via the addition of dopants or composites is the most successful technique. In comparison to other photocatalysts, ZnO is a better photocatalyst in terms of cost and availability, according to the literature review. ZnO was modified to make it more efficient at degrading dye compounds and other pollutants. Apart from that, the degradation efficiency is highly dependent on pH, illumination, temperature, dopant concentration, catalyst dose, and dye concentration. It is also worth noting that ZnO has a higher dye breakdown efficiency when exposed to sunlight, making it a better candidate for investigations. The use of ZnO as a photocatalyst to degrade pollutants, such as dyes, is a potential technology for future development. It is projected that interest in ZnO will continue to increase, resulting in the discovery of novel applications for the material.

Author Contributions: Conceptualization, S.M., Y.A., S.H.K. and C.T.S.; Data curation, Y.A., D.D. and S.H.K., methodology, Y.A., I.H.A. and S.-u.R., validation, K.K.Y., C.T.S. and B.-H.J., formal analysis, A.G., C.T.S. and I.H.A.; resources, K.K.Y., B.-H.J. and I.H.A.; writing—original draft preparation, V.K.Y., S.M., D.D. and S.H.K., writing—review and editing, A.G., V.K.Y., I.H.A., C.T.S., Y.A., S.-u.R. and S.H.K., supervision, V.K.Y., S.M. and B.-H.J., project administration V.K.Y. and K.K.Y., Funding acquisition, B.-H.J., S.-u.R., I.H.A. and A.G., Investigation, V.K.Y., B.-H.J. and S.M., Software's, D.D., C.T.S., S.M., A.G. and K.K.Y., Visualization, A.G., S.-u.R. and B.-H.J. All authors have read and agreed to the published version of the manuscript.

Funding: The authors extend their appreciation to the Deanship of Scientific Research at King Khalid University for funding this work through research groups program under grant number R.G.P. 2/84/43. This work was supported by the Mid-Career Research Program [grant number 2020R1A2C3004237] of the National Research Foundation of the Republic of Korea.

Institutional Review Board Statement: Not applicable.

Data Availability Statement: No separate data are there.

Conflicts of Interest: The authors declare no conflict of interest. All authors have read and agreed to the published version of the manuscript.

Abbreviations

AC	Activated Charcoal
AOPs	Advanced Oxidation Process
BBD	Box–Behnken Design
BOD	Biological Oxygen Demand
CB	Conduction Band
CETP	Common Effluent Treatment Plant
COD	Chemical Oxygen Demand
CTP	Conventional Treatment Process
DLS	Dynamic Light Scattering
EPS	Exopolysaccharides
ERP	Emerging Removal Process
FE-SEM	Field Emission Scanning Electron Microscope
FTIR	Fourier Transform Infrared Spectroscopy
GC-MS	Gas Chromatography-Mass spectroscopy
GIDC	Gujarat Industrial Development Corporation
LD	Lethal Dose
L-H	Langmuir Hinshelwood
MAO	Monoamine Oxidase
MB	Methylene Blue
MBR	Membrane bioreactor
NF	Nanofiltration
NPs	Nanoparticles

PL	Photoluminescence
PUF	Polyurethane Foam
PVP	Polyvinylpyrrolidone
RSM	Response Surface Methodology
SMP	Soluble Microbial Products
TEM	Transmission Electron Microscope
TiO ₂	Titanium Dioxide
TOC	Total organic carbon
UF	Ultrafiltration
UV	Ultraviolet
VB	Valance Band
XRD	X-ray Diffraction
ZnO	Zinc Oxide

References

- Malhi, Y.; Franklin, J.; Seddon, N.; Solan, M.; Turner, M.G.; Field, C.B.; Knowlton, N. Climate change and ecosystems: Threats, opportunities and solutions. *Philos. Trans. R. Soc. B Biol. Sci.* **2020**, *375*, 20190104. [[CrossRef](#)] [[PubMed](#)]
- Lellis, B.; Fávaro-Polonio, C.Z.; Pamphile, J.A.; Polonio, J.C. Effects of textile dyes on health and the environment and bioremediation potential of living organisms. *Biotechnol. Res. Innov.* **2019**, *3*, 275–290. [[CrossRef](#)]
- Berradi, M.; Hsissou, R.; Khudhair, M.; Assouag, M.; Cherkaoui, O.; El Bachiri, A.; El Harfi, A. Textile finishing dyes and their impact on aquatic environs. *Heliyon* **2019**, *5*, e02711. [[CrossRef](#)] [[PubMed](#)]
- Slama, H.B.; Chenari Bouket, A.; Pourhassan, Z.; Alenezi, F.N.; Silini, A.; Cherif-Silini, H.; Oszako, T.; Luptakova, L.; Golińska, P.; Belbahri, L. Diversity of Synthetic Dyes from Textile Industries, Discharge Impacts and Treatment Methods. *Appl. Sci.* **2021**, *11*, 6255. [[CrossRef](#)]
- Sarkar, S.; Banerjee, A.; Halder, U.; Biswas, R.; Bandopadhyay, R. Degradation of Synthetic Azo Dyes of Textile Industry: A Sustainable Approach Using Microbial Enzymes. *Water Conserv. Sci. Eng.* **2017**, *2*, 121–131. [[CrossRef](#)]
- Shindhal, T.; Rakholiya, P.; Varjani, S.; Pandey, A.; Ngo, H.H.; Guo, W.; Ng, H.Y.; Taherzadeh, M.J. A critical review on advances in the practices and perspectives for the treatment of dye industry wastewater. *Bioengineered* **2021**, *12*, 70–87. [[CrossRef](#)]
- Mohanan, N.; Montazer, Z.; Sharma, P.K.; Levin, D.B. Microbial and Enzymatic Degradation of Synthetic Plastics. *Front. Microbiol.* **2020**, *11*, 2837. [[CrossRef](#)]
- Briffa, J.; Sinagra, E.; Blundell, R. Heavy metal pollution in the environment and their toxicological effects on humans. *Heliyon* **2020**, *6*, e04691. [[CrossRef](#)]
- Sankaranarayanan, A.; Karthikeyan, S.; Markande, A.; Sharma, A. Remazol reactive dye degrading Bacteria from freshwater fish of River Cauvery, Pallipalayam of Namakkal District, South India. *Environ. Syst. Res.* **2021**, *10*, 29. [[CrossRef](#)]
- Adegoke, K.A.; Bello, O.S. Dye sequestration using agricultural wastes as adsorbents. *Water Resour. Ind.* **2015**, *12*, 8–24. [[CrossRef](#)]
- Mohammed, N.; Lian, H.; Islam, M.S.; Strong, M.; Shi, Z.; Berry, R.M.; Yu, H.-Y.; Tam, K.C. Selective adsorption and separation of organic dyes using functionalized cellulose nanocrystals. *Chem. Eng. J.* **2021**, *417*, 129237. [[CrossRef](#)]
- Yusuf, M.; Shabbir, M.; Mohammad, F. Natural Colorants: Historical, Processing and Sustainable Prospects. *Nat. Prod. Bioprospect.* **2017**, *7*, 123–145. [[CrossRef](#)] [[PubMed](#)]
- Aggarwal, S. Indian dye yielding plants: Efforts and opportunities. *Nat. Resour. Forum* **2021**, *45*, 63–86. [[CrossRef](#)]
- Wisniewska, M.; Wawrzekiewicz, M.; Onyszko, M.; Medykowska, M.; Nosal-Wiercinska, A.; Bogatyrov, V. Carbon-Silica Composite as Adsorbent for Removal of Hazardous C.I. Basic Yellow 2 and C.I. Basic Blue 3 Dyes. *Materials* **2021**, *14*, 3245. [[CrossRef](#)]
- Yaseen, D.A.; Scholz, M. Textile dye wastewater characteristics and constituents of synthetic effluents: A critical review. *Int. J. Environ. Sci. Technol.* **2019**, *16*, 1193–1226. [[CrossRef](#)]
- Ardila-Leal, L.D.; Poutou-Pinales, R.A.; Pedroza-Rodriguez, A.M.; Quevedo-Hidalgo, B.E. A Brief History of Colour, the Environmental Impact of Synthetic Dyes and Removal by Using Laccases. *Molecules* **2021**, *26*, 3813. [[CrossRef](#)]
- Yadav, V.K.; Khan, S.H.; Choudhary, N.; Tirth, V.; Kumar, P.; Ravi, R.K.; Modi, S.; Khayal, A.; Shah, M.P.; Sharma, P.; et al. Nanobioremediation: A sustainable approach towards the degradation of sodium dodecyl sulfate in the environment and simulated conditions. *J. Basic Microbiol.* **2022**, *62*, 348–360. [[CrossRef](#)]
- Nyankson, E.; Adjasoo, J.; Efavi, J.K.; Amedalor, R.; Yaya, A.; Manu, G.P.; Asare, K.; Amartey, N.A. Characterization and Evaluation of Zeolite A/Fe₃O₄ Nanocomposite as a Potential Adsorbent for Removal of Organic Molecules from Wastewater. *J. Chem.* **2019**, *2019*, 8090756. [[CrossRef](#)]
- Nizam, N.U.M.; Hanafiah, M.M.; Mahmoudi, E.; Halim, A.A.; Mohammad, A.W. The removal of anionic and cationic dyes from an aqueous solution using biomass-based activated carbon. *Sci. Rep.* **2021**, *11*, 8623. [[CrossRef](#)]
- Njanja, E.; Mbokou, S.F.; Pontie, M.; Nacef, M.; Tonle, I.K. Comparative assessment of methylene blue biosorption using coffee husks and corn cobs: Towards the elaboration of a lignocellulosic-based amperometric sensor. *SN Appl. Sci.* **2019**, *1*, 513. [[CrossRef](#)]
- Lee, Y.S.; Wurster, R.D. Methylene blue induces cytotoxicity in human brain tumor cells. *Cancer Lett.* **1995**, *88*, 141–145. [[CrossRef](#)]

22. Al-Fawwaz, A.T.; Abdullah, M. Decolorization of Methylene Blue and Malachite Green by Immobilized *Desmodesmus* sp. Isolated from North Jordan. *Int. J. Environ. Sci. Dev.* **2016**, *7*, 95–99. [[CrossRef](#)]
23. Durão, C.; Pedrosa, F.; Dinis-Oliveira, R.J. Greenish-blue discoloration of the brain and heart after treatment with methylene blue. *Forensic Sci. Med. Pathol.* **2021**, *17*, 148–151. [[CrossRef](#)]
24. Salhab, M.; Al Sarakbi, W.; Mokbel, K. Skin and fat necrosis of the breast following methylene blue dye injection for sentinel node biopsy in a patient with breast cancer. *Int. Semin. Surg. Oncol.* **2005**, *2*, 26. [[CrossRef](#)]
25. Luis-Silva, F.; Meneguetti, M.G.; Sepeda, C.D.R.; Petroski-Moraes, B.C.; Sato, L.; Peres, L.M.; Becari, C.; Basile-Filho, A.; Evora, P.R.B.; Martins-Filho, O.A.; et al. Effect of methylene blue on hemodynamic and metabolic response in septic shock patients. *Medicine* **2022**, *101*, e28599. [[CrossRef](#)] [[PubMed](#)]
26. Clifton, J., II; Leikin, J.B. Methylene Blue. *Am. J. Ther.* **2003**, *10*, 289–291. [[CrossRef](#)]
27. Dewachter, P.; Mouton-Faivre, C.; Tréchet, P.; Lléu, J.-C.; Mertes, P.M. Severe Anaphylactic Shock with Methylene Blue Instillation. *Anesth. Analg.* **2005**, *101*, 149–150. [[CrossRef](#)]
28. Koyande, A.K.; Chew, K.W.; Rambabu, K.; Tao, Y.; Chu, D.-T.; Show, P.-L. Microalgae: A potential alternative to health supplementation for humans. *Food Sci. Hum. Wellness* **2019**, *8*, 16–24. [[CrossRef](#)]
29. Singh, A.; Sharma, R.; Pant, D.; Malaviya, P. Engineered algal biochar for contaminant remediation and electrochemical applications. *Sci. Total Environ.* **2021**, *774*, 145676. [[CrossRef](#)]
30. Butler, E.; Hung, Y.-T.; Yeh, R.Y.-L.; Suleiman Al Ahmad, M. Electrocoagulation in Wastewater Treatment. *Water* **2011**, *3*, 495–525. [[CrossRef](#)]
31. Crini, G. Non-conventional low-cost adsorbents for dye removal: A review. *Bioresour. Technol.* **2006**, *97*, 1061–1085. [[CrossRef](#)] [[PubMed](#)]
32. Pirkarami, A.; Olya, M.E. Removal of dye from industrial wastewater with an emphasis on improving economic efficiency and degradation mechanism. *J. Saudi Chem. Soc.* **2017**, *21*, S179–S186. [[CrossRef](#)]
33. Alizadeh, M.; Ghahramani, E.; Zarrabi, M.; Hashemi, S. Efficient De-colorization of Methylene Blue by Electro-coagulation Method: Comparison of Iron and Aluminum Electrode. *Iran. J. Chem. Chem. Eng.-Int.* **2015**, *34*, 39–47.
34. Mahmoud, M.S.; Farah, J.Y.; Farrag, T.E. Enhanced removal of Methylene Blue by electrocoagulation using iron electrodes. *Egypt. J. Pet.* **2013**, *22*, 211–216. [[CrossRef](#)]
35. de Carvalho, H.P.; Huang, J.; Zhao, M.; Liu, G.; Dong, L.; Liu, X. Improvement of Methylene Blue removal by electrocoagulation/banana peel adsorption coupling in a batch system. *Alex. Eng. J.* **2015**, *54*, 777–786. [[CrossRef](#)]
36. Zhang, D.H.; Yang, H.M.; Ou, Y.J.; Xu, C.; Gu, J.C. Treatment of printing and dyeing wastewater by catalytic wet hydrogen peroxide oxidation of honeycomb cinder as carrier catalyst. *IOP Conf. Ser. Earth Environ. Sci.* **2017**, *69*, 012039. [[CrossRef](#)]
37. Anirudhan, T.S.; Ramachandran, M. Adsorptive removal of basic dyes from aqueous solutions by surfactant modified bentonite clay (organoclay): Kinetic and competitive adsorption isotherm. *Process Saf. Environ. Prot.* **2015**, *95*, 215–225. [[CrossRef](#)]
38. Ullah, H.; Nafees, M.; Iqbal, F.; Awan, S.; Shah, A.; Waseem, A. Adsorption kinetics of malachite green and methylene blue from aqueous solutions using surfactant-modified organoclays. *Acta Chim. Slov.* **2017**, *64*, 449–460. [[CrossRef](#)]
39. Ponnusami, V.; Madhuram, R.; Krithika, V.; Srivastava, S.N. Effects of process variables on kinetics of methylene blue sorption onto untreated guava (*Psidium guajava*) leaf powder: Statistical analysis. *Chem. Eng. J.* **2008**, *140*, 609–613. [[CrossRef](#)]
40. Foo, K.Y.; Hameed, B.H. Potential of jackfruit peel as precursor for activated carbon prepared by microwave induced NaOH activation. *Bioresour. Technol.* **2012**, *112*, 143–150. [[CrossRef](#)]
41. Hameed, B.H.; El-Khaiary, M.I. Batch removal of malachite green from aqueous solutions by adsorption on oil palm trunk fibre: Equilibrium isotherms and kinetic studies. *J. Hazard. Mater.* **2008**, *154*, 237–244. [[CrossRef](#)] [[PubMed](#)]
42. Hameed, B.H.; Krishni, R.R.; Sata, S.A. A novel agricultural waste adsorbent for the removal of cationic dye from aqueous solutions. *J. Hazard. Mater.* **2009**, *162*, 305–311. [[CrossRef](#)] [[PubMed](#)]
43. Bendaho, D.; Driss, T.A.; Bassou, D. Adsorption of acid dye onto activated Algerian clay. *Bull. Chem. Soc. Ethiop.* **2017**, *31*, 51–62. [[CrossRef](#)]
44. Chowdhury, S.; Mishra, R.; Kushwaha, P.; Saha, P. Removal of safranin from aqueous solutions by NaOH-treated rice husk: Thermodynamics, kinetics and isosteric heat of adsorption. *Asia-Pac. J. Chem. Eng.* **2012**, *7*, 236–249. [[CrossRef](#)]
45. Muthuraman, G.; Teng, T.T.; Leh, C.P.; Norli, I. Extraction and recovery of methylene blue from industrial wastewater using benzoic acid as an extractant. *J. Hazard. Mater.* **2009**, *163*, 363–369. [[CrossRef](#)] [[PubMed](#)]
46. Pandit, P.; Basu, S. Removal of Ionic Dyes from Water by Solvent Extraction Using Reverse Micelles. *Environ. Sci. Technol.* **2004**, *38*, 2435–2442. [[CrossRef](#)] [[PubMed](#)]
47. Belisti Lelisa, M.M. Removal of Methylene Blue (Mb) Dye from Aqueous Solution by Bioadsorption onto Untreated *Parthenium hysterophorus* Weed. *Mod. Chem. Appl.* **2014**, *2*, 146. [[CrossRef](#)]
48. Al Abdallah, Q.; Choe, S.-I.; Campoli, P.; Baptista, S.; Gravelat, F.N.; Lee, M.J.; Sheppard, D.C. A Conserved C-Terminal Domain of the *Aspergillus fumigatus* Developmental Regulator MedA Is Required for Nuclear Localization, Adhesion and Virulence. *PLoS ONE* **2012**, *7*, e49959. [[CrossRef](#)]
49. Eslami, H.; Sedighi Khavidak, S.; Salehi, F.; Khosravi, R.; Fallahzadeh, R.A.; Peirovi, R.; Sadeghi, S. Biodegradation of methylene blue from aqueous solution by bacteria isolated from contaminated soil. *J. Adv. Environ. Health Res.* **2017**, *5*, 10–15. [[CrossRef](#)]

50. Singh, R.; Pathak, B.; Fulekar, M.H. Characterization of PGP Traits by Heavy Metals Tolerant *Pseudomonas putida* and *Bacillus safensis* Strain Isolated from Rhizospheric Zone of Weed (*Phyllanthus urinaria*) and its efficiency in Cd and Pb Removal. *Int. J. Curr. Microbiol. App. Sci.* **2015**, *4*, 954–975.
51. Fulekar, M.H.; Wadgaonkar, S.L.; Singh, A. Decolourization of Dye Compounds by Selected Bacterial Strains isolated from Dyestuff Industrial Area. *Int. J. Adv. Res. Technol.* **2013**, *2*, 182–192.
52. Vijayaraghavan, K.; Mao, J.; Yun, Y.-S. Biosorption of methylene blue from aqueous solution using free and polysulfone-immobilized *Corynebacterium glutamicum*: Batch and column studies. *Bioresour. Technol.* **2008**, *99*, 2864–2871. [[CrossRef](#)] [[PubMed](#)]
53. Ranade, V.V.; Bhandari, V.M. Chapter 1—Industrial Wastewater Treatment, Recycling, and Reuse: An Overview. In *Industrial Wastewater Treatment, Recycling and Reuse*; Ranade, V.V., Bhandari, V.M., Eds.; Butterworth-Heinemann: Oxford, UK, 2014; pp. 1–80. [[CrossRef](#)]
54. Yadav, V.K.; Khan, S.H.; Malik, P.; Thappa, A.; Suriyaprabha, R.; Ravi, R.K.; Choudhary, N.; Kalasariya, H.; Gnanamoorthy, G. Microbial Synthesis of Nanoparticles and Their Applications for Wastewater Treatment. In *Microbial Biotechnology: Basic Research and Applications*; Singh, J., Vyas, A., Wang, S., Prasad, R., Eds.; Springer: Singapore, 2020; pp. 147–187. [[CrossRef](#)]
55. Khan, S.H.; Yadav, V.K. Advanced Oxidation Processes for Wastewater Remediation: An Overview. In *Removal of Emerging Contaminants Through Microbial Processes*; Shah, M.P., Ed.; Springer: Singapore, 2021; pp. 71–93. [[CrossRef](#)]
56. Jo, W.-K.; Tayade, R.J. Recent developments in photocatalytic dye degradation upon irradiation with energy-efficient light emitting diodes. *Chin. J. Catal.* **2014**, *35*, 1781–1792. [[CrossRef](#)]
57. Fetimi, A.; Merouani, S.; Khan, M.S.; Asghar, M.N.; Yadav, K.K.; Jeon, B.-H.; Hamachi, M.; Kebiche-Senhadji, O.; Benguerba, Y. Modeling of Textile Dye Removal from Wastewater Using Innovative Oxidation Technologies (Fe(II)/Chlorine and H₂O₂/Periodate Processes): Artificial Neural Network-Particle Swarm Optimization Hybrid Model. *ACS Omega* **2022**, *7*, 13818–13825. [[CrossRef](#)]
58. Zhao, Q.; Li, N.; Liao, C.; Tian, L.; An, J.; Wang, X. The UV/H₂O₂ process based on H₂O₂ in-situ generation for water disinfection. *J. Hazard. Mater. Lett.* **2021**, *2*, 100020. [[CrossRef](#)]
59. Kurian, M. Advanced oxidation processes and nanomaterials—A review. *Clean. Eng. Technol.* **2021**, *2*, 100090. [[CrossRef](#)]
60. Tijani, J.O.; Fatoba, O.O.; Madzivire, G.; Petrik, L.F. A Review of Combined Advanced Oxidation Technologies for the Removal of Organic Pollutants from Water. *Water Air Soil Pollut.* **2014**, *225*, 2102. [[CrossRef](#)]
61. Pawar, M.; Topcu Sendogdular, S.; Gouma, P. A Brief Overview of TiO₂ Photocatalyst for Organic Dye Remediation: Case Study of Reaction Mechanisms Involved in Ce-TiO₂ Photocatalysts System. *J. Nanomater.* **2018**, *2018*, 5953609. [[CrossRef](#)]
62. Karunakaran, C.; Senthilvelan, S. Photocatalysis with ZrO₂: Oxidation of aniline. *J. Mol. Catal. A Chem.* **2005**, *233*, 1–8. [[CrossRef](#)]
63. Gnanaprakasam, A.; Sivakumar, V.M.; Thirumarimurugan, M. Influencing Parameters in the Photocatalytic Degradation of Organic Effluent via Nanometal Oxide Catalyst: A Review. *Indian J. Mater. Sci.* **2015**, *2015*, 601827. [[CrossRef](#)]
64. Molinari, R.; Lavorato, C.; Argurio, P. Visible-Light Photocatalysts and Their Perspectives for Building Photocatalytic Membrane Reactors for Various Liquid Phase Chemical Conversions. *Catalysts* **2020**, *10*, 1334. [[CrossRef](#)]
65. Ibadon, A.O.; Fitzpatrick, P. Heterogeneous Photocatalysis: Recent Advances and Applications. *Catalysts* **2013**, *3*, 189–218. [[CrossRef](#)]
66. Azeez, F.; Al-Hetlani, E.; Arafa, M.; Abdelmonem, Y.; Nazeer, A.A.; Amin, M.O.; Madkour, M. The effect of surface charge on photocatalytic degradation of methylene blue dye using chargeable titania nanoparticles. *Sci. Rep.* **2018**, *8*, 7104. [[CrossRef](#)] [[PubMed](#)]
67. Schirripa Spagnolo, G.; Leccese, F.; Leccisi, M. LED as Transmitter and Receiver of Light: A Simple Tool to Demonstration Photoelectric Effect. *Crystals* **2019**, *9*, 531. [[CrossRef](#)]
68. Kang, X.; Liu, S.; Dai, Z.; He, Y.; Song, X.; Tan, Z. Titanium Dioxide: From Engineering to Applications. *Catalysts* **2019**, *9*, 191. [[CrossRef](#)]
69. Mammadov, J.; Buyyarapu, R.; Guttikonda, S.K.; Parliament, K.; Abdurakhmonov, I.Y.; Kumpatla, S.P. Wild Relatives of Maize, Rice, Cotton, and Soybean: Treasure Troves for Tolerance to Biotic and Abiotic Stresses. *Front. Plant Sci.* **2018**, *9*, 886. [[CrossRef](#)]
70. Pirkanniemi, K.; Sillanpää, M. Heterogeneous water phase catalysis as an environmental application: A review. *Chemosphere* **2002**, *48*, 1047–1060. [[CrossRef](#)]
71. Ma, S.; Xue, J.; Zhou, Y.; Zhang, Z. Photochemical synthesis of ZnO/Ag₂O heterostructures with enhanced ultraviolet and visible photocatalytic activity. *J. Mater. Chem. A* **2014**, *2*, 7272–7280. [[CrossRef](#)]
72. Ribeiro, D.; Freitas, M.; Lima, J.L.F.C.; Fernandes, E. Proinflammatory Pathways: The Modulation by Flavonoids. *Med. Res. Rev.* **2015**, *35*, 877–936. [[CrossRef](#)]
73. Adeleke, J.T.; Theivasanthi, T.; Thiruppathi, M.; Swaminathan, M.; Akomolafe, T.; Alabi, A.B. Photocatalytic degradation of methylene blue by ZnO/NiFe₂O₄ nanoparticles. *Appl. Surf. Sci.* **2018**, *455*, 195–200. [[CrossRef](#)]
74. Houas, A.; Lachheb, H.; Ksibi, M.; Elaloui, E.; Guillard, C.; Herrmann, J.M. Photocatalytic degradation pathway of methylene blue in water. *Appl. Catal. B Environ.* **2001**, *31*, 145–157. [[CrossRef](#)]
75. Reza, K.M.; Kurny, A.S.W.; Gulshan, F. Parameters affecting the photocatalytic degradation of dyes using TiO₂: A review. *Appl. Water Sci.* **2017**, *7*, 1569–1578. [[CrossRef](#)]
76. Mir, S.A.; Bhat, J.I.A.; Lone, F.; Rehman, M.U.; Nazir, N.; Lone, A.A.; Ali, T.; Jehangir, A. Synergistic effects of vehicular emissions (NO₂, SO₂ and SPM) on progression of *Crocus sativus* L. in Saffron bowl Kashmir. *Environ. Adv.* **2021**, *3*, 100033. [[CrossRef](#)]

77. Palmisano, L.; García-López, E.I.; Marci, G. Inorganic materials acting as heterogeneous photocatalysts and catalysts in the same reactions. *Dalton Trans.* **2016**, *45*, 11596–11605. [[CrossRef](#)]
78. Ali, H.R.; Motawea, E.A. Ternary Photodegradable Nanocomposite (BiOBr/ZnO/WO₃) for the Degradation of Phenol Pollutants: Optimization and Experimental Design. *ACS Omega* **2021**, *6*, 22047–22064. [[CrossRef](#)]
79. Tesfay Mulu, Z.; Kirk Amber, C.; Hadac Elizabeth, M.; Griesmann Guy, E.; Federspiel Mark, J.; Barber Glen, N.; Henry Stephen, M.; Peng, K.-W.; Russell Stephen, J. PEGylation of Vesicular Stomatitis Virus Extends Virus Persistence in Blood Circulation of Passively Immunized Mice. *J. Virol.* **2013**, *87*, 3752–3759. [[CrossRef](#)]
80. Chen, R.; Li, D.; Liu, B.; Peng, Z.; Gurzadyan, G.G.; Xiong, Q.; Sun, H. Optical and Excitonic Properties of Crystalline ZnS Nanowires: Toward Efficient Ultraviolet Emission at Room Temperature. *Nano Lett.* **2010**, *10*, 4956–4961. [[CrossRef](#)]
81. Espitia, P.J.P.; Soares, N.d.F.F.; Coimbra, J.S.d.R.; de Andrade, N.J.; Cruz, R.S.; Medeiros, E.A.A. Zinc Oxide Nanoparticles: Synthesis, Antimicrobial Activity and Food Packaging Applications. *Food Bioprocess Technol.* **2012**, *5*, 1447–1464. [[CrossRef](#)]
82. Menad, A.; Benmalti, M.E.; Zaoui, A.; Ferhat, M. Impact of polytypism on the ground state properties of zinc oxide: A first-principles study. *Results Phys.* **2020**, *18*, 103316. [[CrossRef](#)]
83. Han, C.; Yang, M.-Q.; Weng, B.; Xu, Y.-J. Improving the photocatalytic activity and anti-photocorrosion of semiconductor ZnO by coupling with versatile carbon. *Phys. Chem. Chem. Phys.* **2014**, *16*, 16891–16903. [[CrossRef](#)]
84. Jayappa, M.D.; Ramaiah, C.K.; Kumar, M.A.P.; Suresh, D.; Prabhu, A.; Devasya, R.P.; Sheikh, S. Green synthesis of zinc oxide nanoparticles from the leaf, stem and in vitro grown callus of *Mussaenda frondosa* L.: Characterization and their applications. *Appl. Nanosci.* **2020**, *10*, 3057–3074. [[CrossRef](#)] [[PubMed](#)]
85. Agarwal, H.; Venkat Kumar, S.; Rajeshkumar, S. A review on green synthesis of zinc oxide nanoparticles—An eco-friendly approach. *Resour.-Effic. Technol.* **2017**, *3*, 406–413. [[CrossRef](#)]
86. Iravani, S.; Korbekandi, H.; Mirmohammadi, S.V.; Zolfaghari, B. Synthesis of silver nanoparticles: Chemical, physical and biological methods. *Res. Pharm. Sci.* **2014**, *9*, 385–406. [[PubMed](#)]
87. Zhang, X.-F.; Liu, Z.-G.; Shen, W.; Gurunathan, S. Silver Nanoparticles: Synthesis, Characterization, Properties, Applications, and Therapeutic Approaches. *Int. J. Mol. Sci.* **2016**, *17*, 1534. [[CrossRef](#)]
88. Iravani, S. Bacteria in Nanoparticle Synthesis: Current Status and Future Prospects. *Int. Sch. Res. Not.* **2014**, *2014*, 359316. [[CrossRef](#)]
89. Shah, M.; Fawcett, D.; Sharma, S.; Tripathy, S.K.; Poinern, G.E.J. Green Synthesis of Metallic Nanoparticles via Biological Entities. *Materials* **2015**, *8*, 7278–7308. [[CrossRef](#)]
90. Sutradhar, P.; Saha, M. Silver Nanoparticles: Synthesis and Its Nanocomposites for Heterojunction Polymer Solar Cells. *J. Phys. Chem. C* **2016**, *120*, 8941–8949. [[CrossRef](#)]
91. Siddiqi, K.S.; Husen, A. Plant Response to Engineered Metal Oxide Nanoparticles. *Nanoscale Res. Lett.* **2017**, *12*, 92. [[CrossRef](#)]
92. Himanen, L.; Geurts, A.; Foster, A.S.; Rinke, P. Data-Driven Materials Science: Status, Challenges, and Perspectives. *Adv. Sci.* **2019**, *6*, 1900808. [[CrossRef](#)]
93. Anbuvarannan, M.; Ramesh, M.; Viruthagiri, G.; Shanmugam, N.; Kannadasan, N. Synthesis, characterization and photocatalytic activity of ZnO nanoparticles prepared by biological method. *Spectrochim. Acta Part A Mol. Biomol. Spectrosc.* **2015**, *143*, 304–308. [[CrossRef](#)]
94. Ledakowicz, S.; Paździar, K. Recent Achievements in Dyes Removal Focused on Advanced Oxidation Processes Integrated with Biological Methods. *Molecules* **2021**, *26*, 870. [[CrossRef](#)] [[PubMed](#)]
95. Contreras, M.; Grande-Tovar, C.D.; Vallejo, W.; Chaves-López, C. Bio-Removal of Methylene Blue from Aqueous Solution by *Galactomyces geotrichum* KL20A. *Water* **2019**, *11*, 282. [[CrossRef](#)]
96. Bhawana, P.; Fulekar, M.H. Bioremediation of Dyestuff Compounds using Indigenous Microorganism in a Bioreactor. *APCBEE Procedia* **2012**, *1*, 27–33. [[CrossRef](#)]
97. Chauhan, H.A.; Rafatullah, M.; Ali, K.A.; Umar, M.F.; Khan, M.A.; Jeon, B.-H. Photocatalytic activity of graphene oxide/zinc oxide nanocomposite derived from rice husk for the degradation of phenanthrene under ultraviolet-visible light. *J. Water Process Eng.* **2022**, *47*, 102714. [[CrossRef](#)]
98. Ashun, E.; Kang, W.; Thapa, B.S.; Gurung, A.; Rahimnejad, M.; Jang, M.; Jeon, B.-H.; Kim, J.R.; Oh, S.-E. A novel gas production bioassay of thiosulfate utilizing denitrifying bacteria (TUDB) for the toxicity assessment of heavy metals contaminated water. *Chemosphere* **2022**, *303*, 134902. [[CrossRef](#)]
99. Chavan, A.; Fulekar, M.H. Integration of Photocatalytic Oxidation and Biodegradation Treatment Processes to Enhance Degradation Efficiency of CETP Wastewater Contaminants. *BioNanoScience* **2018**, *8*, 761–768. [[CrossRef](#)]
100. Baker, S.; Perianova, O.V.; Prudnikova, S.V.; Kuzmin, A.; Potkina, N.K.; Khohlova, O.Y.; Lobova, T.I. Phytogenic Nanoparticles to Combat Multi Drug Resistant Pathogens and Photocatalytic Degradation of Dyes. *BioNanoScience* **2020**, *10*, 486–492. [[CrossRef](#)]
101. Yogalakshmi, K.N.; Das, A.; Rani, G.; Jaswal, V.; Randhawa, J.S. Nano-bioremediation: A New Age Technology for the Treatment of Dyes in Textile Effluents. In *Bioremediation of Industrial Waste for Environmental Safety: Volume I: Industrial Waste and Its Management*; Saxena, G., Bharagava, R.N., Eds.; Springer: Singapore, 2020; pp. 313–347. [[CrossRef](#)]
102. Aber, S.; Mahmoudikia, E.; Karimi, A.; Mahdizadeh, F. Immobilization of Glucose Oxidase on Fe₃O₄ Magnetic Nanoparticles and its Application in the Removal of Acid Yellow 12. *Water Air Soil Pollut.* **2016**, *227*, 93. [[CrossRef](#)]
103. Nithya, R.; Ragnathan, R. Synthesis of silver nanoparticle using *Pleurotus sajor caju* and its antimicrobial study. *Dig. J. Nanomater. Biostruct.* **2009**, *4*, 623–629.

104. Hynes, N.R.J.; Kumar, J.S.; Kamyab, H.; Sujana, J.A.J.; Al-Khashman, O.A.; Kuslu, Y.; Ene, A.; Suresh Kumar, B. Modern enabling techniques and adsorbents based dye removal with sustainability concerns in textile industrial sector—A comprehensive review. *J. Clean. Prod.* **2020**, *272*, 122636. [[CrossRef](#)]
105. Khan, S.H.; Pathak, B.; Fulekar, M.H. A study on the influence of metal (Fe, Bi, and Ag) doping on structural, optical, and antimicrobial activity of ZnO nanostructures. *Adv. Compos. Hybrid Mater.* **2020**, *3*, 551–569. [[CrossRef](#)]
106. Nagar, A.; Pradeep, T. Clean Water through Nanotechnology: Needs, Gaps, and Fulfillment. *ACS Nano* **2020**, *14*, 6420–6435. [[CrossRef](#)] [[PubMed](#)]
107. Abul, A.; Samad, S.; Huq, D.; Moniruzzaman, M.; Masum, M. Textile Dye Removal from Wastewater Effluents Using Chitosan-ZnO Nanocomposite. *J. Text. Sci. Eng.* **2015**, *05*, 200. [[CrossRef](#)]
108. Hairom, N.H.H.; Mohammad, A.W.; Ng, L.Y.; Kadhum, A.A.H. Utilization of self-synthesized ZnO nanoparticles in MPR for industrial dye wastewater treatment using NF and UF membrane. *Desalination Water Treat.* **2015**, *54*, 944–955. [[CrossRef](#)]
109. Sidik, D.A.B.; Hairom, N.H.H.; Zainuri, N.Z.; Desa, A.L.; Misdan, N.; Yusof, N.; Ong, C.B.; Mohammad, A.W.; Aripin, N.S.M. Photocatalytic Degradation of Industrial Dye Wastewater Using Zinc Oxide-Polyvinylpyrrolidone Nanoparticles. *Malays. J. Anal. Sci.* **2018**, *22*, 693–701. [[CrossRef](#)]
110. Inderyas, A.; Bhatti, I.A.; Ashar, A.; Ashraf, M.; Ghani, A.; Yousaf, M.; Mohsin, M.; Ahmad, M.; Rafique, S.; Masood, N.; et al. Synthesis of immobilized ZnO over polyurethane and photocatalytic activity evaluation for the degradation of azo dye under UV and solar light irradiation. *Mater. Res. Express* **2020**, *7*, 025033. [[CrossRef](#)]
111. Sheik Mydeen, S.; Raj Kumar, R.; Kottaisamy, M.; Vasantha, V.S. Biosynthesis of ZnO nanoparticles through extract from *Prosopis juliflora* plant leaf: Antibacterial activities and a new approach by rust-induced photocatalysis. *J. Saudi Chem. Soc.* **2020**, *24*, 393–406. [[CrossRef](#)]
112. Balcha, A.; Yadav, O.P.; Dey, T. Photocatalytic degradation of methylene blue dye by zinc oxide nanoparticles obtained from precipitation and sol-gel methods. *Environ. Sci. Pollut. Res.* **2016**, *23*, 25485–25493. [[CrossRef](#)]
113. Gnanamoorthy, G.; Yadav, V.K.; Ali, D.; Narayanan, V.; Mohammed Saleh Katubi, K.; Alarifi, S. Trigger action of copper aminophosphate (X-CuAP) nanoparticles for enhanced electrochemical, photocatalyst and biological properties. *Opt. Mater.* **2021**, *117*, 111113. [[CrossRef](#)]
114. Dworschak, D.; Brunnhofer, C.; Valtiner, M. Photocorrosion of ZnO Single Crystals during Electrochemical Water Splitting. *ACS Appl. Mater. Interfaces* **2020**, *12*, 51530–51536. [[CrossRef](#)]
115. Altıntug, E.; Yenigun, M.; Sari, A.; Altundag, H.; Tuzen, M.; Saleh, T.A. Facile synthesis of zinc oxide nanoparticles loaded activated carbon as an eco-friendly adsorbent for ultra-removal of malachite green from water. *Environ. Technol. Innov.* **2021**, *21*, 101305. [[CrossRef](#)]
116. Gnanamoorthy, G.; Ramar, K.; Padmanaban, A.; Yadav, V.K.; Suresh Babu, K.; Karthikeyan, V.; Narayanan, V. Implementation of ZnSnO₃ nanosheets and their RE (Er, Eu, and Pr) materials: Enhanced photocatalytic activity. *Adv. Powder Technol.* **2020**, *31*, 1209–1219. [[CrossRef](#)]
117. Liang, Z.; Yan, C.-F.; Rtimi, S.; Bandara, J. Piezoelectric materials for catalytic/photocatalytic removal of pollutants: Recent advances and outlook. *Appl. Catal. B Environ.* **2019**, *241*, 256–269. [[CrossRef](#)]
118. Khalafi, T.; Buazar, F.; Ghanemi, K. Phycosynthesis and Enhanced Photocatalytic Activity of Zinc Oxide Nanoparticles Toward Organosulfur Pollutants. *Sci. Rep.* **2019**, *9*, 6866. [[CrossRef](#)] [[PubMed](#)]
119. Chauhan, A.; Verma, R.; Kumari, S.; Sharma, A.; Shandilya, P.; Li, X.; Batoo, K.M.; Imran, A.; Kulshrestha, S.; Kumar, R. Photocatalytic dye degradation and antimicrobial activities of Pure and Ag-doped ZnO using *Cannabis sativa* leaf extract. *Sci. Rep.* **2020**, *10*, 7881. [[CrossRef](#)] [[PubMed](#)]
120. Gnanamoorthy, G.; Ali, D.; Yadav, V.K.; Dhinakaran, G.; Venkatachalam, K.; Narayanan, V. New construction of Fe₃O₄/rGO/ZnSnO₃ nanocomposites enhanced photoelectro chemical properties. *Opt. Mater.* **2020**, *109*, 110353. [[CrossRef](#)]
121. Kumar, U.; Nabgan, W.; Martis, P.; Sreenivasa, S.; Sharma, S.C.; Raghu, M.S.; Alsalmeh, A.; Akshatha, S.; Jeon, B.-H.; Parashuram, L. NrGO wrapped Cu-ZrO₂ as a multifunctional visible-light-sensitive catalyst for advanced oxidation of pollutants and CO₂ reduction. *J. Environ. Chem. Eng.* **2022**, *10*, 107679.
122. Kong, J.-Z.; Li, A.-D.; Li, X.-Y.; Zhai, H.-F.; Zhang, W.-Q.; Gong, Y.-P.; Li, H.; Wu, D. Photo-degradation of methylene blue using Ta-doped ZnO nanoparticle. *J. Solid State Chem.* **2010**, *183*, 1359–1364. [[CrossRef](#)]
123. Zhang, D.; Zeng, F. Visible light-activated cadmium-doped ZnO nanostructured photocatalyst for the treatment of methylene blue dye. *J. Mater. Sci.* **2012**, *47*, 2155–2161. [[CrossRef](#)]
124. Omid, A.; Habibi-Yangjeh, A. Microwave-assisted method for preparation of Sb-doped ZnO nanostructures and their photocatalytic activity. *J. Iran. Chem. Soc.* **2014**, *11*, 457–465. [[CrossRef](#)]
125. Shirini, F.; Abedini, M.; Zamani, S.; Fallah Moafi, H. Introduction of W-doped ZnO nanocomposite as a new and efficient nanocatalyst for the synthesis of biscoumarins in water. *J. Nanostruct. Chem.* **2015**, *5*, 123–130. [[CrossRef](#)]
126. Sanoop, P.K.; Anas, S.; Ananthakumar, S.; Gunasekar, V.; Saravanan, R.; Ponnusami, V. Synthesis of yttrium doped nanocrystalline ZnO and its photocatalytic activity in methylene blue degradation. *Arab. J. Chem.* **2016**, *9*, S1618–S1626. [[CrossRef](#)]
127. Hemalatha, P.; Karthick, S.N.; Hemalatha, K.V.; Yi, M.; Kim, H.-J.; Alagar, M. La-doped ZnO nanoflower as photocatalyst for methylene blue dye degradation under UV irradiation. *J. Mater. Sci. Mater. Electron.* **2016**, *27*, 2367–2378. [[CrossRef](#)]
128. Bhatia, S.; Verma, N.; Bedi, R.K. Optical application of Er-doped ZnO nanoparticles for photodegradation of direct red-31 dye. *Opt. Mater.* **2016**, *62*, 392–398. [[CrossRef](#)]

129. Hemalatha, K.; Manivel, A.; Kumar, M.S.; Mohan, S.C. Synthesis and Characterization of Sn/ZnO Nanoparticles for Removal of Organic Dye and Heavy Metal. *Int. J. Biol. Chem.* **2017**, *12*, 1–7. [[CrossRef](#)]
130. Zandsalimi, Y.; Shahmoradi, B.; Dehestani Athar, S.; Maleki, A. Hydrothermal synthesis and characterization of Tungsten-doped ZnO nanoparticles as an environmentally friendly substance. *J. Adv. Environ. Health Res.* **2018**, *6*, 173–178. [[CrossRef](#)]
131. Vallejo, W.; Cantillo, A.; Díaz-Urbe, C. Methylene Blue Photodegradation under Visible Irradiation on Ag-Doped ZnO Thin Films. *Int. J. Photoenergy* **2020**, *2020*, 1627498. [[CrossRef](#)]
132. Vignesh, K.; Rajarajan, M.; Suganthi, A. Visible light assisted photocatalytic performance of Ni and Th co-doped ZnO nanoparticles for the degradation of methylene blue dye. *J. Ind. Eng. Chem.* **2014**, *20*, 3826–3833. [[CrossRef](#)]
133. Gnanamoorthy, G.; Priya, P.; Ali, D.; Lakshmi, M.; Yadav, V.K.; Varghese, R. A new CuZr₂S₄/rGO and their reduced graphene oxide nanocomposites enhanced photocatalytic and antimicrobial activities. *Chem. Phys. Lett.* **2021**, *781*, 139011. [[CrossRef](#)]
134. Yadav, V.K.; Malik, P.; Khan, A.H.; Pandit, P.R.; Hasan, M.A.; Cabral-Pinto, M.M.S.; Islam, S.; Suriyaprabha, R.; Yadav, K.K.; Dinis, P.A.; et al. Recent Advances on Properties and Utility of Nanomaterials Generated from Industrial and Biological Activities. *Crystals* **2021**, *11*, 634. [[CrossRef](#)]
135. Okpala, C.C. Nanocomposites—An Overview. *Int. J. Eng. Res. Dev.* **2013**, *8*, 17–23.
136. Pirhashemi, M.; Habibi-Yangjeh, A. Photosensitization of ZnO by AgBr and Ag₂CO₃: Nanocomposites with tandem n-n heterojunctions and highly enhanced visible-light photocatalytic activity. *J. Colloid Interface Sci.* **2016**, *474*, 103–113. [[CrossRef](#)] [[PubMed](#)]
137. Saravanan, R.; Gupta, V.K.; Mosquera, E.; Gracia, F. Preparation and characterization of V₂O₅/ZnO nanocomposite system for photocatalytic application. *J. Mol. Liq.* **2014**, *198*, 409–412. [[CrossRef](#)]
138. Nourmoradi, H.; Ghiasvand, A.R.; Noorimotlagh, Z. Removal of methylene blue and acid orange 7 from aqueous solutions by activated carbon coated with zinc oxide (ZnO) nanoparticles: Equilibrium, kinetic, and thermodynamic study. *Desalination Water Treat.* **2015**, *55*, 252–262. [[CrossRef](#)]
139. Nasir, M.; Irnamera, D.; Zulfikar, M.A. Synthesis and characterization of novel TiO₂-ZnO-CoO nanocomposite photocatalyst for photodegradation of methylene blue dye. *IOP Conf. Ser. Earth Environ. Sci.* **2017**, *60*, 012015. [[CrossRef](#)]
140. Darvishi Cheshmeh Soltani, R.; Jorfi, S.; Ramezani, H.; Purfadakari, S. Ultrasonically induced ZnO–biosilica nanocomposite for degradation of a textile dye in aqueous phase. *Ultrason. Sonochem.* **2016**, *28*, 69–78. [[CrossRef](#)]
141. Prasanna, L.; Rajagopalan, V. A New Synergetic Nanocomposite for Dye Degradation in Dark and Light. *Sci. Rep.* **2016**, *6*, 38606. [[CrossRef](#)]
142. Patil, S.P.; Shrivastava, V.S.; Sonawane, G.H. Photocatalytic degradation of Rhodamine 6G using ZnO-montmorillonite nanocomposite: A kinetic approach. *Desalination Water Treat.* **2015**, *54*, 374–381. [[CrossRef](#)]
143. Hosseini, S.A.; Babaei, S. Graphene Oxide/Zinc Oxide (GO/ZnO) Nanocomposite as a Superior Photocatalyst for Degradation of Methylene Blue (MB)-Process Modeling by Response Surface Methodology (RSM). *J. Braz. Chem. Soc.* **2016**, *28*, 299–307. [[CrossRef](#)]
144. Wang, H.; Zhou, P.; Guo, R.; Wang, Y.; Zhan, H.; Yuan, Y. Synthesis of Rectorite/Fe₃O₄/ZnO Composites and Their Application for the Removal of Methylene Blue Dye. *Catalysts* **2018**, *8*, 107. [[CrossRef](#)]
145. Ritika; Kaur, M.; Umar, A.; Mehta, S.K.; Singh, S.; Kansal, S.K.; Fouad, H.; Allothman, O.Y. Rapid Solar-Light Driven Superior Photocatalytic Degradation of Methylene Blue Using MoS₂-ZnO Heterostructure Nanorods Photocatalyst. *Materials* **2018**, *11*, 2254. [[CrossRef](#)] [[PubMed](#)]
146. Munawaroh, H.; Sari, P.L.; Wahyuningsih, S.; Ramelan, A.H. The photocatalytic degradation of methylene blue using graphene oxide (GO)/ZnO nanodrums. *AIP Conf. Proc.* **2018**, *2014*, 020119. [[CrossRef](#)]
147. Micheal, K.; Ayeshamariam, A.; Devanesan, S.; Bhuvaneshwari, K.; Pazhanivel, T.; AlSalhi, M.S.; Aljaafreh, M.J. Environmental friendly synthesis of carbon nanoplates supported ZnO nanorods for enhanced degradation of dyes and organic pollutants with visible light driven photocatalytic performance. *J. King Saud Univ.—Sci.* **2020**, *32*, 1081–1087. [[CrossRef](#)]
148. Lee, J.-E.; Khoa, N.T.; Kim, S.W.; Kim, E.J.; Hahn, S.H. Fabrication of Au/GO/ZnO composite nanostructures with excellent photocatalytic performance. *Mater. Chem. Phys.* **2015**, *164*, 29–35. [[CrossRef](#)]
149. Daneshvar, N.; Salari, D.; Khataee, A.R. Photocatalytic degradation of azo dye acid red 14 in water on ZnO as an alternative catalyst to TiO₂. *J. Photochem. Photobiol. A Chem.* **2004**, *162*, 317–322. [[CrossRef](#)]
150. Chakrabarti, S.; Dutta, B.K. Photocatalytic degradation of model textile dyes in wastewater using ZnO as semiconductor catalyst. *J. Hazard. Mater.* **2004**, *112*, 269–278. [[CrossRef](#)]
151. Byrappa, K.; Subramani, A.K.; Ananda, S.; Rai, K.M.L.; Dinesh, R.; Yoshimura, M. Photocatalytic degradation of rhodamine B dye using hydrothermally synthesized ZnO. *Bull. Mater. Sci.* **2006**, *29*, 433–438. [[CrossRef](#)]
152. Behnajady, M.A.; Modirshahla, N.; Hamzavi, R. Kinetic study on photocatalytic degradation of C.I. Acid Yellow 23 by ZnO photocatalyst. *J. Hazard. Mater.* **2006**, *133*, 226–232. [[CrossRef](#)]
153. Pare, B.; Jonnalagadda, S.B.; Tomar, H.; Singh, P.; Bhagwat, V.W. ZnO assisted photocatalytic degradation of acridine orange in aqueous solution using visible irradiation. *Desalination* **2008**, *232*, 80–90. [[CrossRef](#)]
154. Salem, I.A.; Salem, M.A.; El-Ghobashy, M.A. The dual role of ZnO nanoparticles for efficient capture of heavy metals and Acid blue 92 from water. *J. Mol. Liq.* **2017**, *248*, 527–538. [[CrossRef](#)]
155. Aminuzzaman, M.; Ying, L.P.; Goh, W.-S.; Watanabe, A. Green synthesis of zinc oxide nanoparticles using aqueous extract of *Garcinia mangostana* fruit pericarp and their photocatalytic activity. *Bull. Mater. Sci.* **2018**, *41*, 50. [[CrossRef](#)]

156. Laouedj, N. ZnO-Assisted Photocatalytic Degradation of Congo Red and Benzopurpurine 4B in Aqueous Solution. *J. Chem. Eng. Process Technol.* **2011**, *2*, 106. [[CrossRef](#)]
157. Amini, M.; Ashrafi, M. Photocatalytic degradation of some organic dyes under solar light irradiation using TiO₂ and ZnO nanoparticles. *Nanochem. Res.* **2016**, *1*, 79–86. [[CrossRef](#)]
158. Salim, H.A.; Salih, S.A.; Rashid, R.A. Removal of Acid Alizarin Black Dye from Aqueous Solution by Adsorption Using Zinc Oxide. *Int. Res. J. Pure Appl. Chem.* **2015**, *11*, 1–8. [[CrossRef](#)]
159. Kumar, R.; Umar, A.; Kumar, G.; Akhtar, M.S.; Wang, Y.; Kim, S.H. Ce-doped ZnO nanoparticles for efficient photocatalytic degradation of direct red-23 dye. *Ceram. Int.* **2015**, *41*, 7773–7782. [[CrossRef](#)]
160. Vivekraj, P.; Gideon, A.V. Enhanced Photocatalytic Degradation Properties of Zinc Oxide Nanoparticles Synthesized by using *Turnera subulata* Sm. *Int. J. Pharm. Res. Sch.* **2018**, *7*, 30–40. [[CrossRef](#)]
161. Meena, S.; Vaya, D.; Das, B.K. Photocatalytic degradation of Malachite Green dye by modified ZnO nanomaterial. *Bull. Mater. Sci.* **2016**, *39*, 1735–1743. [[CrossRef](#)]
162. Lee, H.J.; Kim, J.H.; Park, S.S.; Hong, S.S.; Lee, G.D. Degradation kinetics for photocatalytic reaction of methyl orange over Al-doped ZnO nanoparticles. *J. Ind. Eng. Chem.* **2015**, *25*, 199–206. [[CrossRef](#)]
163. Soltani, R.D.C.; Rezaee, A.; Khataee, A.R.; Safari, M. Photocatalytic process by immobilized carbon black/ZnO nanocomposite for dye removal from aqueous medium: Optimization by response surface methodology. *J. Ind. Eng. Chem.* **2014**, *20*, 1861–1868. [[CrossRef](#)]
164. Jorfi, S.; Barkhordari, M.J.; Ahmadi, M.; Jaafarzadeh, N.; Moustofi, A.; Ramavandi, B. Photodegradation of Acid red 18 dye by BiOI/ZnO nanocomposite: A dataset. *Data Brief* **2018**, *16*, 608–611. [[CrossRef](#)]
165. Nakkeeran, E.; Varjani, S.J.; Dixit, V.; Kalaiselvi, A. Synthesis, characterization and application of zinc oxide nanocomposite for dye removal from textile industrial wastewater. *Indian J. Exp. Biol.* **2018**, *56*, 498–503.